nature reviews earth & environment

https://doi.org/10.1038/s43017-025-00735-1

Review article

Check for updates

Earth's past and present mantle oxygen fugacity

Elizabeth Cottrell [1] ✉, Dante Canil [2], Charles Langmuir [3], Katy A. Evans [4] & Fabrice Gaillard [5]

Abstract

Oxygen is the most abundant element in Earth's mantle. Oxygen fugacity (fO_2), which quantifies the availability of oxygen to mediate oxidation–reduction reactions, affects important mantle processes, such as depth of melting, extraction of volatiles to the atmosphere, crustal composition and ore body generation. Debate continues over modern and past variations in mantle fO_2. In this Review, we compile thermobarometric data from mafic and ultramafic rocks at ridges, back-arcs, and arcs and show that the fO_2 of subduction-influenced arc mantle is appreciably higher than the mantle supplying ocean ridges. We review the timing and mechanisms that might transfer redox budget to the arc mantle wedge. A new proxy for the redox-sensitive element vanadium confirms the higher oxidation state of arc mantle and can be used to show there is no conclusive evidence for oxidation of the ambient mantle since the Archaean (2,500–4,000 million years ago). Earlier, in the Hadean magma ocean (>4,000 million years ago), liquid silicate equilibrated with liquid metal alloy while the upper mantle was rapidly oxidized to higher fO_2. Future research should focus on how mantle fO_2 coevolved with Earth's primitive atmosphere during core formation, magma ocean crystallization and degassing.

Sections

[1]Department of Mineral Sciences, National Museum of Natural History, Smithsonian Institution, Washington DC, Washington DC, USA. [2]School of Earth and Ocean Sciences, University of Victoria, Victoria, British Columbia, Canada. [3]Department of Earth and Planetary Sciences, Harvard University, Cambridge, MA, USA. [4]Curtin Frontier Institute for Geoscience Solutions, School of Earth and Planetary Sciences, Curtin University, Perth, Australia. [5]Institut des Sciences de la Terre d'Orléans, CNRS/Université d'Orléans/BRGM, Orléans, France.
✉e-mail: cottrellE@si.edu

Key points

- Oxybarometric and vanadium-based proxies reveal that the oxygen fugacity (fO_2) of mid-ocean ridge basalts and ridge peridotites < back-arc basin basalts < arc basalts and peridotites. The fO_2 of plume sources is difficult to constrain, varied and cannot be generalized.
- The elevated fO_2 of basalts and peridotites in subduction zones can be related to the local influence of the subducting slab within only 1–2 Myr of subduction initiation.
- A range of possible mechanisms might contribute to the link between subduction and elevated mantle fO_2. Existing data suggest sulfur has the greatest potential to transfer the elevated redox budget of subducting slabs to the mantle wedge.
- Application of trace element proxies reconfirms that Earth's bulk mantle $Fe^{3+}/\Sigma Fe$ has not substantially increased since the Archaean (4 billion years ago). Gradual or sudden changes in mantle $Fe^{3+}/\Sigma Fe$ are unlikely to have enabled the Great Oxidation Event.
- Evolution of mantle fO_2 during and just after the Hadean magma ocean is key to understanding mechanisms for mantle oxidation.

Introduction

The oxygen fugacity (fO_2) (Box 1) of Earth's present-day mantle, as set by the activity–composition relationships (Box 2) of mantle minerals and melts, is important for modelling key geodynamic variables, such as the depth of the mantle solidus[1–3], production and composition of Earth's crust[4–6], speciation of mantle-derived fluids and gases[7], and the formation of ore[8,9,10] and diamondiferous[11] deposits. The formation of Earth's core[12,13] and first atmosphere[14–16] also relate to Earth's initial planetary redox balance, which is now anchored by Earth's mantle and mantle-derived melts.

Petrologists in the latter half of the twentieth century developed numerous oxybarometers and proxies to assess the fO_2 of igneous systems, inclusive of peridotites[17,18], basalts[19], komatiites[20], and more evolved rocks, such as granites[5] and rhyolites[21]. Since the turn of the twenty-first century, new analytical and experimental techniques, oxybarometers and proxies, and activity–composition models have come into use, leading to a proliferation of new observations and debate about the modern spatial variation and ancient history of mantle fO_2. A critical assessment of the resultant wealth of data is timely and needed.

Subduction zones serve as a tectonic nexus for transfer of redox budget (Box 2) between Earth's interior and exterior reservoirs[22,23]. Although it has long been recognized that mid-ocean ridge basalts (MORB) and peridotites record lower fO_2 than subduction-influenced lavas and xenoliths[24–26], vigorous debate has emerged over whether arc lavas are oxidized by mantle or crustal processes[27–31].

However, it is clear that subduction-influenced basalts record higher fO_2 than MORB — even shortly after subduction initiation[32,33]. Identifying the lithologies and elements that enable the redox budget to transfer from the subducting slab to the wedge has therefore become a very active area of community investigation and debate[34].

How mantle fO_2 might have changed over time is also debated. It is widely accepted that Earth's core separated from a magma ocean with fO_2 values approximately five orders of magnitude more reducing than present[12]. Controversy centres on when and how the mantle evolved to its more oxidized present state. Evidence that mantle fO_2 has been constant since the Archaean (for example, refs. 20,35–37) led the community to develop mantle oxidation mechanisms integral to the process of core formation[13,16,38,39]. Others have suggested that the ambient mantle underwent oxidation (increasing its bulk fraction of ferric iron relative to the total iron, $Fe^{3+}/\Sigma Fe = Fe^{3+}/[Fe^{3+} + Fe^{2+}]$) during the Archaean, even to the extent that it triggered the Great Oxidation Event (GOE) recorded at Earth's surface[40–42].

In this Review, we compile and synthesize various observations bearing on the Earth's present-day and ancient ambient convecting upper mantle fO_2, from the Hadean to the present, and discuss the potential processes that drive changes in mantle fO_2. We begin the Review in the modern (present-day) mantle, which is well-sampled, comparing mantle fO_2 in different tectonic settings. We continue by reviewing the timing and candidate elements and lithologies that might transfer redox budget to the present-day arc mantle wedge. We then show the temporal variation of mantle fO_2 since the Archaean using observational mantle fO_2 proxies. Last, we outline the multicomponent redox-sensitive processes operating in the Hadean between the core, magma ocean and primordial atmosphere. Related topics, such as redox measurement techniques[43] and fO_2 across the solar system[44] in the continental lithosphere[11,39] and in the lower mantle[39], are not covered here, as they have been well discussed in the previous reviews.

Oxybarometry of present-day mantle

Iron (Fe) is an abundant, multivalent, rock-forming element whose oxidation state can both determine and respond to the fO_2 of geological systems[45]. The fO_2 recorded by submarine pillow glass and olivine-hosted melt (glass) inclusions can be estimated from measurements of Fe valence states. The fO_2 recorded by peridotites and more evolved lavas can be estimated from mineral compositions. All calculations of fO_2 from compositional data require an activity–composition model (Box 2). This section discusses the fO_2 recorded by mantle-derived rocks from 171 localities in different present-day tectonic settings (Supplementary Note 1, Supplementary Table 1).

Oxybarometry of mid-ocean ridges

There is now widespread consensus that MORB records fO_2 within approximately 1 log unit of the quartz–fayalite–magnetite (QFM) buffer[46–48] (Box 1). However, there is great debate about the relative abundances of Fe^{3+} and Fe^{2+} in natural and synthesized mafic glasses equilibrated at the same fO_2 that stems from debate about the interpretation of Mössbauer spectroscopy and wet chemical analyses. For example, determinations for the average $Fe^{3+}/\Sigma Fe$ of MORB range from near 0.08–0.14 (refs. 46,47,49,50).

Assuming that mantle melts are in equilibrium with their solid peridotite mineral residues, the fO_2 of melts and residues must be equivalent at the time of solid–liquid segregation. Melts that decompress without reequilibration with peridotite, for example, in chemically isolated dunite channels[51], will decompress approximately parallel to the QFM buffer[19] (Box 1). However, the relationship between the fO_2 of the MORB-source mantle and the $Fe^{3+}/\Sigma Fe$ ratio of the solid convecting mantle is poorly known[52,53]. Values for the latter range from ~0.03–0.04 based on measurements of xenoliths[54] and MORB[47], to 0.05 from models constrained by experimental petrology[52], to 0.06 based on thermodynamic and empirical calculations[55]. Ridge peridotites — which are the residues of melt extraction — record fO_2 variations over several

Box 1 | fO_2, oxybarometry and redox budget

Fugacity (f) is closely related to chemical activity (a). These variables are used in thermodynamic calculations as proxies for concentration, accounting for non-ideal interactions. Oxygen fugacity (fO_2) is an intensive variable that quantifies the extent to which elements in solid, liquid or vapour phases occur in different valence states.

The change in standard state Gibbs free energy ($\Delta G^0_{reaction}$) of any equilibria involving O_2 can be related to fO_2 via the equilibrium constant (K_{eq}). For example, equation (1) defines the quartz–fayalite–magnetite (QFM) buffer reaction of 3 fayalite ($Fe_2^{2+}SiO_4$)+O_2⟶3 quartz(SiO_2)+2 magnetite ($Fe_2^{3+}Fe^{2+}O_4$). At equilibrium,

$$\Delta G^0_{reaction} = -RT\ln K_{eq} = -RT\ln \frac{\left(a^{quartz}_{SiO_2}\right)^3 \left(a^{spinel}_{Fe_3O_4}\right)^2}{\left(a^{olivine}_{Fe_2SiO_4}\right)^3 fO_2}, \quad (1)$$

where T is temperature, and R is the gas constant. For pure phases, such equilibria define, or 'buffer', the activity and fugacity of O_2 when pressure and temperature are specified. Petrologists often describe the fO_2 of systems relative to a buffer, for example, '1 log unit above QFM' or ΔQFM+1.

Oxybarometry combines mineral compositional information with thermodynamic descriptions of activity–composition relationships (for example, the activity of magnetite in spinel, $a^{spl}_{Fe_3O_4}$) and expressions such as equation 1 to calculate fO_2. The relative fO_2 of common buffers change little with temperature but diverge with changing pressure. For example, along an adiabat, basalt decompresses approximately parallel to QFM, whereas spinel-peridotite decompresses approximately parallel to the fayalite–ferrosilite–magnetite (FFM) buffer.

Redox budget is an extensive variable defined as the number of electrons required to bring the redox-sensitive elements in a rock to a reference state defined for the system of interest. Generally, reference states of Fe such as Fe^{2+}, O as O^{2-}, C as C^0 and S as S^{2-} are appropriate for the study of subarc mantle because these elements are dominantly held in these valence states within the mantle[125]. Rocks with all elements in the reference redox state have a redox budget of zero; more oxidized rocks are likely to have redox budgets greater than zero.

Redox budget changes with the amount of material whereas fO_2 is independent of quantity. A rock consisting of 99% magnetite (Fe_3O_4) and 1% hematite (Fe_2O_3) has a much greater redox budget than a rock consisting of 50% of each, but the fO_2 of both rocks lies on the hematite–magnetite (HM) buffer. Intensive variables change in a nonlinear way when oxidants or reductants are added, so it is difficult to use fO_2 to measure fluxes of oxidizing or reducing material. The use of redox budget to measure the transfer of oxidants or reductants resolves this issue[22,249].

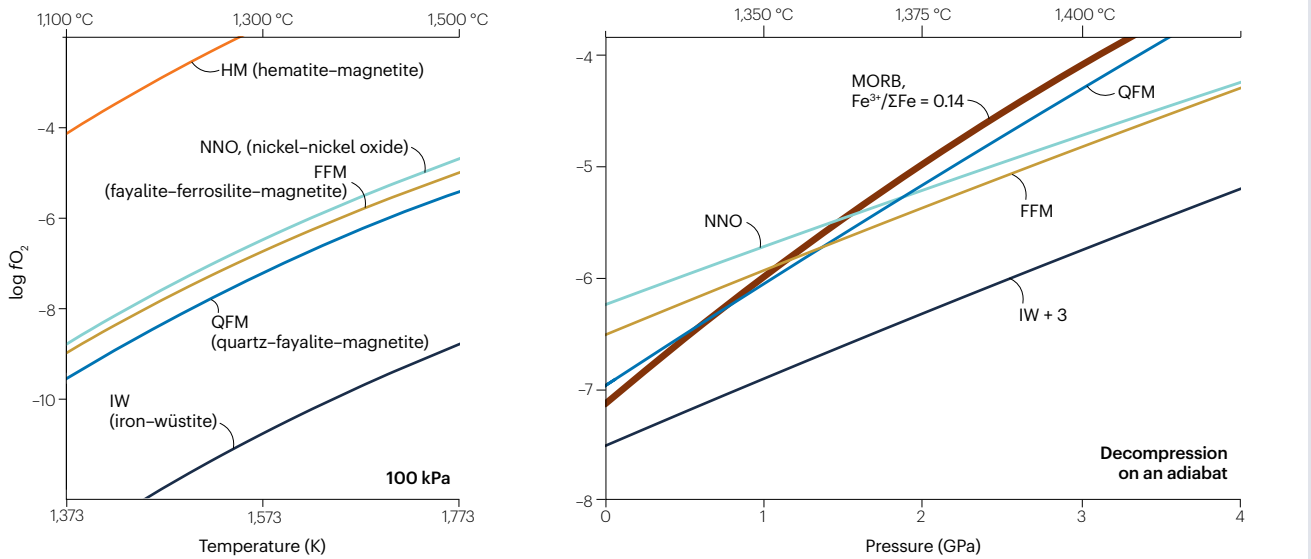

orders of magnitude higher and lower than QFM[56–58], even at the scale of a single ridge segment[57]. Although the subsolidus processes that might alter ridge peridotite fO_2 remain an active area of research, these rocks, on average, record fO_2 near QFM, consistent with the basalts they generate[57,59] (Fig. 1a).

That the MORB-source mantle is near QFM, not one or two orders of magnitude lower as previously inferred[56,60], has important implications for the stability of graphite in the mantle and hence the depth and importance of redox melting. For any value of bulk mantle $Fe^{3+}/\Sigma Fe$, fO_2 decreases with depth[26,61]. Because oxidized carbon fluxes mantle melting and reduced carbon does not, the possibility of redox melting in the mantle depends on the depth at which carbonate is reduced to graphite (or diamond), with commensurate oxidation of Fe (ref. 62). The reaction occurs at approximately constant fO_2, independent of depth, such that higher bulk mantle $Fe^{3+}/\Sigma Fe$ ratios increase the plausible depth of carbonated silicate melt generation[1–3]. Many geophysical properties have been attributed to the presence of such low-degree carbonatitic or carbonated silicate melts[3]; hence, the mantle's redox-depth profile has relevance to the interpretation of geophysical observations.

Box 2 | fO_2 and $Fe^{3+}/\Sigma Fe$

Oxygen fugacity (fO_2) and $Fe^{3+}/\Sigma Fe$ are related but not interchangeable. Activity–composition relationships for minerals, fluids and silicate melts allow us to translate between fO_2 and $Fe^{3+}/\Sigma Fe$. Because Fe is an abundant multivalent element, $Fe^{3+}/\Sigma Fe$ is a first-order control on system fO_2.

Consider two assemblages of quartz+fayalite+magnetite, one with molar proportions of quartz:fayalite:magnetite of 0.2:0.7:0.1 and the other 0.2:0.1:0.7. Both assemblages are at log fO_2 ΔQFM (quartz–fayalite–magnetite) of 0. The former has $Fe^{3+}/\Sigma Fe$ of 0.06, whereas the latter has $Fe^{3+}/\Sigma Fe$ of 0.44, illustrating that whole rock $Fe^{3+}/\Sigma Fe$ cannot be equated to fO_2 based on assemblage alone. Similarly, although thermodynamic calculations suggest that mantle peridotite with bulk $Fe^{3+}/\Sigma Fe$ of 0.03 equilibrates with a basaltic melt with $Fe^{3+}/\Sigma Fe$ three to five times higher, we lack experimentally constrained activity–composition models to relate the $Fe^{3+}/\Sigma Fe$ of erupted basalts to the $Fe^{3+}/\Sigma Fe$ of their unmelted peridotitic mantle sources[52,53]. This is true, even though the fO_2 of mid-ocean ridge basalt is well known.

When comparing basalts of similar composition, $Fe^{3+}/\Sigma Fe$ is a good, if imperfect, proxy for relative fO_2. However, for melts with disparate compositions, $Fe^{3+}/\Sigma Fe$ must always be related to fO_2 via an activity–composition model that takes into consideration the major element composition of the melt, the temperature and the pressure (panel **b** constructed using refs. 19,223,224). For example, the $Fe^{3+}/\Sigma Fe$ value of an alkali-rich melt (for example, phonolite) is higher than that of an alkali-poor melt under the same fO_2 conditions.

The fO_2-decompression path of melt-absent peridotite with a constant $Fe^{3+}/\Sigma Fe$ is constrained by xenolith oxybarometry, experiments and thermodynamic models (for example, ref. 58). Large changes in fO_2 are driven primarily by redistribution of Fe^{3+} as the mineral assemblage changes with pressure. Now, consider a liquid magma ocean with a uniform $Fe^{3+}/\Sigma Fe$. At upper mantle pressures, the fO_2 of liquid silicate increases with pressure. However, at extreme pressures (>20 GPa), the trend reverses and melts with high $Fe^{3+}/\Sigma Fe$ coexist with Fe^0 alloys[16] at low fO_2 values.

In summary, neither melts nor solid phase assemblages undergo monotonic changes in fO_2 with pressure. When reporting calculated fO_2, the activity–composition models and buffer formulations must be referenced.

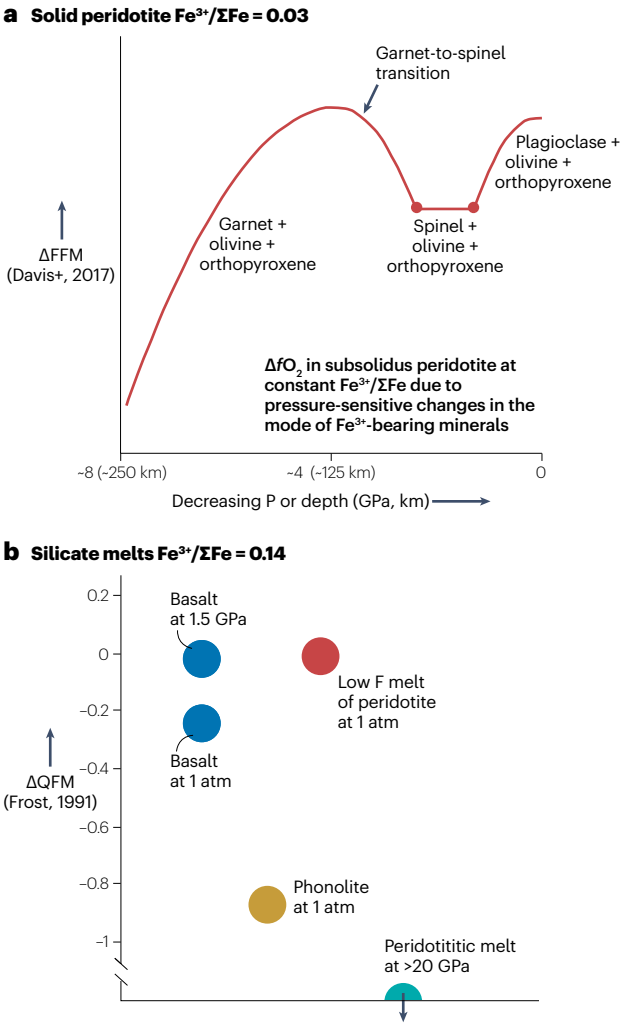

Xenoliths have been instrumental in establishing the redox-depth profile of the continents[39], but ridges do not offer xenoliths that would help us to establish the redox-depth profile of the convecting mantle. Observations of peridotites[54,58,59], MORB[47,50,63] and experimental determinations of Fe^{3+} partitioning between basalts and peridotite residues[52,64,65] suggest that mineral chemistries and modes might evolve to maintain approximately constant melt $Fe^{3+}/\Sigma Fe$ during mantle melting on a modern adiabat, though this is not universally agreed upon[66]. These preliminary investigations, which were made possible by microbeam advances in the determination of Fe^{3+}, herald continuing advancements.

Thermodynamic models are used to connect the chemistry of melts sampled at the surface to the coevolving melts and residues present at depth. The applicability of thermodynamic model frameworks, such as MELTS[67] or THERMOCALC[68], to accurate modelling of Fe^{3+}-bearing peridotite and melt systems are still being explored[52,55,58,69,70]. It has become clear that thermodynamic models will require modification to accurately link melt fO_2 to the $Fe^{3+}/\Sigma Fe$ ratio of the solid mantle[52,58,65]. Indeed, additional observations and thermodynamic modelling[52,55,58,69,71] provide constraints — and competing models — on the relationships between melt chemistry and mantle chemistry, temperature and pressure.

Oxybarometry of back arcs and arcs

Most back-arc basin basalts (BABB) record fO_2 from ~QFM to QFM + 1 (refs. 25,30). Arc volcanic rocks of various compositions record fO_2 from just above QFM to ~QFM + 2.5 (ref. 72) and show no systematic variation with major element composition or crustal thickness[72]. Postulated mechanisms to modify the composition of arc magmas include assimilation[27,73,74], crystal fractionation[29,73,75] and degassing[28,76–78]. Crystal fractionation of olivine, which contains only very trace amounts of Fe^{3+}, has a clear but modest potential to raise the fO_2 of MORB by less

than 0.5 log units[47,48]. Crystal fractionation of garnet, which can accommodate substantial amounts of Fe^{3+}, has the potential to raise the fO_2 of arc magmas by just under a log unit after 50% eclogite crystallization[31]. Degassing of S as SO_2 can lead to reduction of >0.25 log units relative fO_2 (refs. 76,77,79). The extent of fO_2 modifications due to degassing depend on the initial fO_2 of the source, the volatile composition of the primary magma and the pressure of quench (or melt inclusion entrapment)[72]. Degassing models predict arc magmas with typical concentrations of C–O–S–H (carbon–oxygen–sulfur–hydrogen) species might become slightly more or less oxidized as they ascend and degas but remain within ~0.2 log units of their source, especially if quenched above 500 bar (ref. 72). The samples less affected by degassing and fractionation, such as primitive (MgO >6 wt.%) and minimally degassed arc basalts[25,30,80] and lower crustal cumulates[81,82], suggest that the source mantle beneath arcs is oxidized, in the range of QFM to QFM + 2, similar to (fore)arc mantle xenoliths[72,83–86] (Fig. 1a).

Despite these robust observations, there has been substantial debate about whether the mantle wedge source of subduction zones is more oxidized or whether oxidation happens during transport to the surface.

Oxybarometry of plumes

The fO_2 of plume-affected lavas (including compositions as diverse as basalt and phonolite) record a wider range of fO_2 than MORB, from QFM − 1 to QFM + 2 (ref. 72), with $Fe^{3+}/\Sigma Fe$ ranging from 0.09 to 0.4 (ref. 87). It is difficult to extract mantle fO_2 from many plume-affected lavas, however, because the latter are often sampled from the subaerial eruptions of ocean islands where degassing is much more extreme than in the submarine environment. For example, once factors such as S degassing are considered, the modelled fO_2 of plume source mantle varies somewhat less, from QFM to QFM + 2 (ref. 87) (Supplementary Table 1).

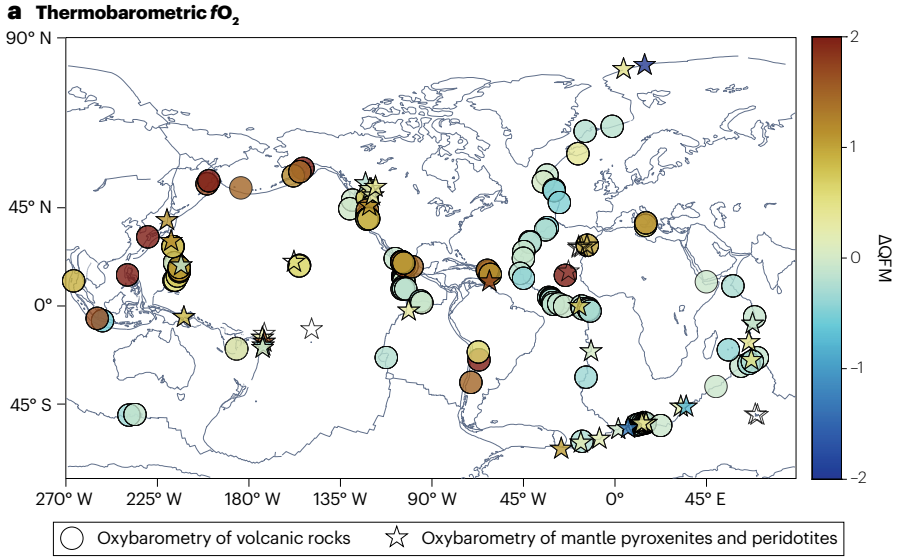

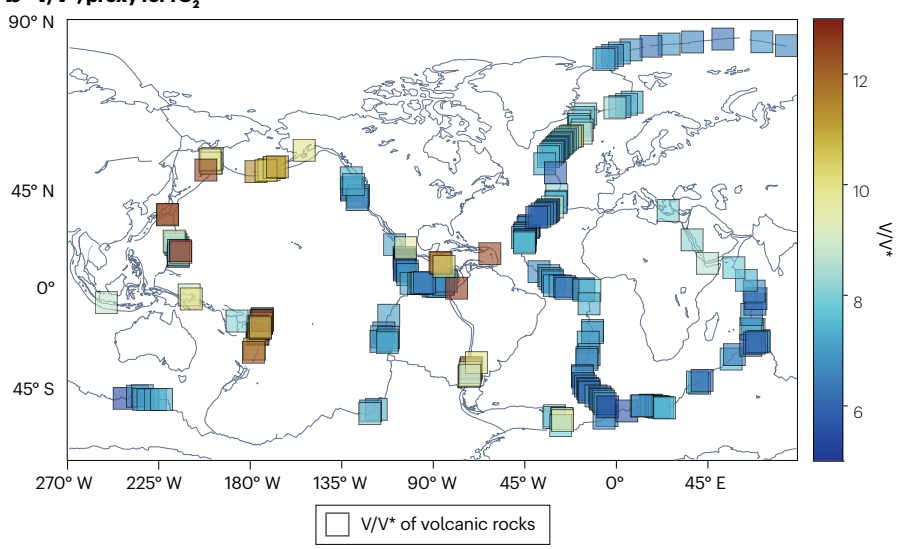

Fig. 1 | Maps of redox data across present-day tectonic settings. a, Average thermobarometric oxygen fugacity (fO_2) recorded by present-day volcanic rocks (circles) and mantle rocks (stars) for localities calculated in ref. 228, which updates ref. 231 (disucssed in ref. 72) with data from refs. 33,80,87,181,232–235 (Supplementary Note 1, Supplementary Table 1). A locality is defined as a ridge segment, volcano, xenolith locality or dredge. Each plume locality is assigned an oxybarometric fO_2 corresponding to the most primitive and least degassed sample using data from refs. 77,79,87,236–239 (Supplementary Table 1). Plume localities with xenolith fO_2 determinations record lithospheric mantle values (open stars). **b**, V/V* (where V* is $Sc^{0.84}*Yb^{0.54}$) for localities calculated in ref. 229 with data from refs. 240–242 (squares). The mantle rocks and primitive basalts in proximity to subduction zones record a higher fO_2 to those distal to subduction zones, and sources proximal to the plumes record variable fO_2. QFM, quartz–fayalite–magnetite.

The fO_2 of plume-affected xenoliths record a wider range of fO_2 than ridge peridotites, from QFM − 2 to QFM + 4 (ref. 72); however, uncertainties on spinel $Fe^{3+}/\Sigma Fe$ — the dominant factor in the calculation of peridotite fO_2 — are very high in this dataset. For example, of the 143 xenoliths (compiled from 13 studies), only 1 study[88] applied Mössbauer-referenced standards for spinel $Fe^{3+}/\Sigma Fe$ during analysis. Even with better measurements, plume xenoliths sample the oceanic lithosphere through which they pass, rather than the residues from the plume source mantle[72]. These various factors make precise determination of plume fO_2 problematic.

Minor and trace elements as fO_2 probes

$Fe^{3+}/\Sigma Fe$ has received the most attention because in many petrological systems it can be used to determine absolute thermobarometric values for fO_2; however, the valence states of multivalent trace elements change in response to fO_2 (for example, as reviewed by ref. 89) and can provide a critical constraint, as discussed in this section.

Vanadium

The incompatible element vanadium (V) exists as V^{2+}, V^{3+}, V^{4+} and V^{5+} in terrestrial systems[90] and is a useful fO_2 proxy. The incompatibility of V^{3+} in mantle minerals is similar to several other trivalent elements, whereas V^{4+} and V^{5+} are more highly incompatible than V^{3+}. If a trivalent cation, herein named V^{3+}_{proxy}, were to behave the same as V^{3+} during peridotite melting, and all V existed as V^{3+} during melting, then the ratio V/V^{3+}_{proxy} of the melt would be constant. Melting peridotite at relatively higher fO_2 should generate basalts with systematically higher melt V concentrations [$V = V^{3+} + V^{4+} + V^{5+}$] compared with V^{3+}_{proxy} and have higher V/V^{3+}_{proxy} concentration ratios. The dependence of V valence state on fO_2 (refs. 20,90) is the conceptual basis of all V-based fO_2 proxies[20,35,41,91].

Trace element concentration-based fO_2 proxies have advantages relative to proxies that rely on measurement of the valence state of an element. First, trace element concentration data are abundant for many lithologies lacking a phase assemblage suitable for oxybarometry (Box 1). Second, if the fO_2 proxies are immobile elements, they might be less easily perturbed by metamorphism, alteration and weathering, or degassing. In this way, trace element concentration proxies might more accurately reveal relative differences in mantle fO_2. However, the absolute accuracy of trace element proxies is model-dependent — being potentially sensitive to factors such as composition, temperature, degree of melting, extent of fractionation and source lithology[6,35,92,93]. In other words, oxybarometry, such as calculated from ilmenite–magnetite[21], spinel-olivine-orthopyroxene[17,18] and glass $Fe^{3+}/\Sigma Fe$ (ref. 24) (Fig. 1a), yields absolute fO_2 directly based on experimentally calibrated activity–composition relationships, whereas trace element methods are most useful as measures of relative fO_2 differences (for example, vanadium-based fO_2 proxy V/V*, where V* is $Sc^{0.84}$*$Yb^{0.54}$, as plotted in Fig. 1b), with further work needed to be able to use them to quantify absolute fO_2.

V/Sc, V/Ti and V/Yb proxies

The most popular trivalent cation to serve as V^{3+}_{proxy} has been Sc. When the V/Sc proxy is applied to mantle-derived basalts, MORB mantle and arc mantle have the same inferred fO_2 (refs. 73,94) (Supplementary Fig. 1). However, the use of Sc is problematic as V^{3+}_{proxy} because Sc is more compatible during spinel-peridotite melting and basalt fractionation than V^{3+} (ref. 93). V/Sc therefore increases as melts fractionate along a liquid line of descent, as can be seen in global data as well as data from a single mid-ocean ridge segment (Fig. 2a). Variations in V/Sc due to variations in extent of melting or crystallization could be misinterpreted as fO_2 variations, and for this reason, ref. 35 recommended filtering data to 8 wt.% < MgO < 12 wt.% before applying V/Sc. For example, metabasalts from <2 billion years ago (Ga) that displayed elevated V/Sc compared with those >2 Ga were interpreted as recording increased mantle fO_2 with time[40]. However, all the data fall on the V/Sc–MgO trend defined by present-day MORB (Fig. 2a).

It has also been suggested that D_V/D_{Sc} for mantle mineral–melt pairs, and hence the V/Sc ratio in rocks, is temperature dependent[92]. However, our analysis of 1-atm data, where fO_2 is precisely measured to better than ±0.05 log units, reveals that $D_V^{olivine/melt}/D_{Sc}^{olivine/melt}$ and $D_V^{clinopyroxene/melt}/D_{Sc}^{clinopyroxene/melt}$ are not significantly temperature dependent (Supplementary Fig. 2 and Supplementary Note 2), consistent with prior work[20,95,96].

V/Yb is less sensitive to crystal fractionation than V/Sc or V/Ti (Supplementary Fig. 1). The V/Yb and V/Ti redox proxies have been applied to lavas across tectonic settings and support conclusions drawn from oxybarometric work; mantle proximal to arcs is more oxidized than at mid-ocean ridges[93,97,98].

V/V*, a new proxy

To refine the utility of V-based redox proxies, the fictive element V* is introduced as a V^{MORB}_{proxy}, where V* is $Sc^{0.84}$*$Yb^{0.54}$. V* is constructed to have geochemical properties intermediate between Sc and Yb such that a regression of V concentrations against V* for glasses dredged from the East Pacific Rise[99] passes through the origin (Supplementary Fig. 1 and Supplementary Note 2). In contrast to V/Sc, V/V* shows no change with MgO (Fig. 2b).

The use of V* does not assume that all V is speciated as V^{3+} during MORB petrogenesis. Rather, V* behaves as V during mantle melting and crystallization of MORB. V/V* is higher than MORB when melting takes place under more oxidizing conditions than the MORB source and lower under conditions more reducing. Application of V* — or any V^{3+}_{proxy} — is complicated when garnet and magnetite are part of the melting or crystallizing assemblage (for example, in plume-derived and some arc-derived basalts) because garnet and magnetite fractionate V from other cations. Therefore, V/V* is applied when rocks are filtered to have MgO >5 wt.% (before magnetite-in) and Dy/Yb <1.8 to eliminate samples with garnet influence[100]. Additional screening criteria are applied to the premodern rock dataset (described below and in Supplementary Note 3).

The sensitivity of V/V* to fO_2, temperature, melt fraction (F), trace element enrichment and depletion in the source, source modal mineralogy, melting reactions and choice of partition coefficients between melt and olivine (ol), clinopyroxene (cpx), orthopyroxene (opx) and spinel is modelled in Supplementary Fig. 3 and Supplementary Note 2. In 1-atm experiments, where fO_2 is measured directly with a sensor, the ratios of partition coefficients, $D_V^{ol/melt}/D_{V*}^{ol/melt}$ and $D_V^{cpx/melt}/D_{V*}^{cpx/melt}$ decrease as fO_2 increases in experimental olivine–melt and clinopyroxene–melt pairs, with no temperature dependence (Fig. 2d and Supplementary Fig. 2). For all model conditions investigated, V/V* is not sensitive to F outside of error from QFM − 1 to QFM + 1; however, at QFM + 2, V/V* falls ~35% as F increases from 0.05 to 0.15, yet does not fall within error of values of QFM + 1 until $F \geq 0.17$ (Fig. 2f). Due to the role of water, F is higher on average at arcs than at ridges[101], making the fO_2 inferred for arc basalts from V/V* likely minima when compared with anhydrous melts such as MORB. Samples with elevated V/V* relative to MORB suggest a more oxidized mantle source, even when the extent of melting (F) differs.

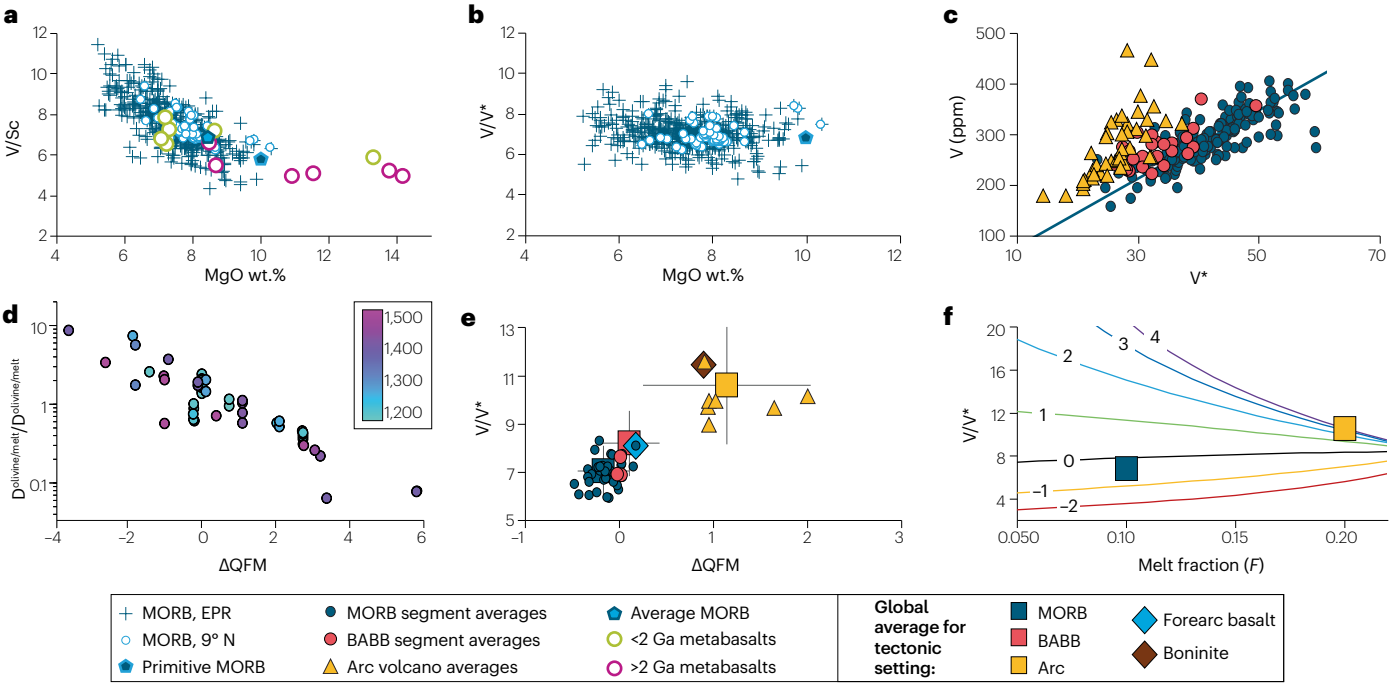

Fig. 2 | V/Sc and V/V* as fO_2 proxies. a, V/Sc as a function of MgO wt.% in East Pacific Rise (EPR) mid-ocean ridge basalts (MORB)[99] (dark blue cross, $n = 872$) and a single segment (EPR29) at 9° N (open circles, $n = 62$) with 5 < MgO < 12 and Dy/Yb <1.8. The green circles and magenta circles are the metabasalts, <2 Ga and >2 Ga, respectively, and the cyan pentagon with the dark blue edge is the average MORB derived in ref. 40. The dark blue pentagon with the cyan edge is the primitive MORB[99]. **b**, V/V* (where V* is $Sc^{0.84}*Yb^{0.54}$) as a function of MgO wt.% with symbols as in **a**. **c**, Segments from global MORB ($n = 185$, dark blue circle) and back-arc basin basalts (BABB) ($n = 24$, pink circle)[243] and arc front volcanoes ($n = 48$, yellow triangle)[30,76,181,241,242] with $n > 2$ samples meeting the V* criteria[229]. **d**, Experimental determinations at 1 atm and temperatures from 1,240 to 1,527 °C of $D_V^{olivine/melt}/D_{V*}^{olivine/melt}$ as a function of oxygen fugacity (fO_2) (refs. 93–96). **e**, Data sources and symbols as in **c** for localities and individual samples where oxybarometric fO_2 (ref. 228 and Supplementary Table 1) and V/V* are both determined. The uncertainty fO_2 calculation is 0.53 log units[72]. Uncertainty in V/V* is a sample-to-sample variation (±1 for ridge segments and from ±0.5 to ±3 for arc volcanoes). The large squares are average V/V* and fO_2 for all samples from a tectonic setting with 1σ error bars (Table 1). **f**, One possible model relationship between V/V* and melt fraction for non-modal melting of a fertile spinel lherzolite source at fO_2 from 2 log units below (red) to 4 log units above (purple) the quartz–fayalite–magnetite (QFM) buffer. fO_2 predicted from V/V* is less process-dependent and model-dependent than that predicted from V/Sc due to the greater sensitivity of V/Sc to melting and crystal fractionation.

The fO_2 predicted from V/V* is not strongly sensitive to source mineralogy (within the range expected for spinel peridotite) or melting reactions; however, when 2% modal spinel is replaced with 2% garnet, V/V* at QFM increases by about a factor of ~2, from 8 to 15. This increase is owing to the strong compatibility of V, Sc and Yb in garnet[102]. The impact of garnet on the relationship between fO_2 and V/V* underscores that V/V* cannot be applied to arc rocks or ocean island rocks where melting in the presence of garnet might be prevalent[103,104].

Results of various additional V/V* sensitivity tests are provided in Supplementary Fig. 3 and Supplementary Note 2. For example, the relationship between fO_2 and V/V* is sensitive to uncertainty in the experimentally determined values of $D_V^{opx/melt}$ and $D_{Sc,Yb}^{cpx/melt}$. Nevertheless, values of V/V* ≥12 yield fO_2 near or above QFM + 1 for all model parameters tested (Supplementary Fig. 3, Supplementary Table 2, Supplementary Table 3). When V/V* >12 and $F > 15\%$, as is true at arcs, fO_2 is constrained to lie above QFM + 1 but could be equally consistent with fO_2 that is several orders of magnitude higher (Fig. 2f). Similar to all trace element proxies, V/V* loses sensitivity at high melt fractions.

These various tests show that V/V* provides a useful assessment of the oxidation states of global mantle-derived lavas. There is a progressive increase of V/V* from MORB to BABB to arc basalts (Fig. 2c, Supplemental Fig. 1). A *t*-test assuming unequal variances shows that the population means (Table 1) are statistically distinct (p values < 0.0001). The increase in V/V* correlates well with independent determinations of fO_2 on the same samples (Supplementary Note 4, Fig. 2e). Because V/V* is not influenced by degassing and is minimally sensitive to other petrogenetic processes, this correlation confirms that these variations are mantle properties and not a result of magma transport. The data demonstrate a strong association of higher V/V* lavas with subduction zone settings compared with mid-ocean ridges (Fig. 1b).

C, S and Cu constraints

Several other trace elements also place constraints on fO_2. For example, the highly incompatible behaviour of C at ridges suggests that MORB mantle is too oxidized (≳QFM − 2) to stabilize graphite, thereby placing a lower bound on MORB-source fO_2 owing to the incompatible behaviour of carbon[105]. Likewise, the fO_2-dependent solubility of S in magmas requires that arc mantle fO_2 must exceed QFM (and the fO_2 of MORB) to reproduce observed arc magma S contents[106–108]. Some arc and back-arc magma S contents also require an S-enriched mantle source,

which would sequester mantle copper (Cu) too efficiently to reproduce arc Cu contents, unless that mantle is relatively oxidized[108–110].

There are therefore multiple lines of evidence that the mantle source of convergent margin (arc and back-arc) basalts are more oxidized than ocean ridges by 1–3 orders of magnitude. Oxybarometric measurements have long shown that arc lavas and mantle peridotites are more oxidized (Fig. 1a). Inferred fO_2 from iron oxidation states and V/V* are broadly correlated across tectonic settings at the locality scale (Fig. 1b) and individual sample scale (Fig. 2e). Arc lava Cu and S contents are not possible unless the arc mantle is more oxidized than MORB mantle. Mantle source fO_2 progressively increases from MORB to BABB to arc as convergent margin influence increases (Fig. 3ab). This debate can now be set to rest.

Subduction-driven oxidation

Oxidation of the mantle wedge increases with increasing slab influence (Fig. 3). The oxidized mantle wedge melts to form volcanic and intrusive rocks at back-arcs and arcs. This section explores the timescales of mantle wedge oxidation and provides an overview of oxidation mechanisms.

Subduction rapidly oxidizes arc mantle

The geochemistry of lavas, tephras and mantle peridotites from arcs records the influence of subducted components, including those that might oxidize the subarc mantle[25,33,80,83,85]. Classic tracers of slab influence in arc magmas, such as Ba/La, Sr/Nd, Th/Yb and Pb/Ce[111,112] correlate with calculated melt fO_2 (Fig. 3a) and V/V* (Fig. 3b) as well as the proportion of S that is isotopically constrained to be slab derived[80,86].

The timescales on which subducted material oxidizes the mantle wedge depend on the concentration, mobility and redox budget of slab components (Box 1); convergence rate; and the volume of mantle involved[23,113,114]. Well-constrained ages of erupted seafloor basalts show that oxidation of the mantle wedge occurs within 1–2 Myr of subduction initiation[32,33] (Fig. 3a).

Oxidation mechanisms at arcs

Once extracted from the mantle, several mechanisms could change the fO_2 of arc magmas. Garnet fractionation could induce oxidation if garnet crystallizes in typical arc crust and if garnet excludes Fe^{3+} (ref. 29). However, laboratory experiments suggest that neither process applies[31,115]. Further, garnet is not on the liquidus for the basaltic compositions considered here, and the heavy rare earth elements do not record garnet fractionation.

In theory, degassing can oxidize or reduce magmas, yet all observations thus far link degassing only to reduction[76,77,79]. Indeed, mineral fractionation, assimilation and degassing can all plausibly modify magma redox, but primitive basalts show little evidence for such modifications[72]. Modification of fO_2 by these processes within the crust must alter the fO_2 of primary magmas equilibrated with arc peridotites, which are 1–3 log units more oxidized than MORB-source mantle (Table 1 and Supplementary Table 1). Therefore, possible mechanisms to oxidize the subarc mantle have received a great deal of attention.

Melts and their magma sources might be oxidized by transport of redox budget[22,23] (Box 1) from the subducted slab to the subarc mantle[8,114,116,117] or indirectly by melting of a source zone modified by the addition of H_2O followed by preferential H_2 loss[118,119]. However, experiments show that H_2O does not affect the melt $Fe^{3+}/\Sigma Fe$ ratio (for example, ref. 120) and mass-balance arguments and mineral compositions provide compelling evidence that H_2O addition to the mantle does not lead to measurable oxidation[121] nor lead to preferential H_2 loss[122]. Therefore, direct transport of elements that carry redox budget is the likely oxidation mechanism.

Elements that transport redox budget

Plausible candidates for transport of redox budget include Fe^{3+} (ref. 117), Mn^{4+} (ref. 123), S_3^- (ref. 124), S^{4+} and S^{6+} (ref. 108), and C^{4+} (ref. 114) because they are present in substantial quantities in the subducting slab, show elevated valence states in the subducting slab relative to those in typical depleted mantle and can occur in sufficient concentrations in aqueous, silicate or supercritical fluids to alter the redox budget of subarc mantle[34,125]. These elements are distributed within sediments, mafic ocean crust and underlying mantle lithosphere[23,114,117] (Fig. 4). Other elements in subducted crust that can have multiple redox states and might be transported from the slab to the subarc mantle, such as

Table 1 | Average oxybarometric fO_2 and geochemistry of localities[a] as a function of tectonic setting and rock type

Age	Tectonic setting and rock type	Average Relative fO_2 (ΔQFM[b])	1σ[c]	Number of localities	Average V/V*	1σ[c]	Number of localities
Present day	Mid-ocean ridge basalt segments	−0.17	0.13	60	7	0.7	185
	Back-arc basin basalt segments	0.03	0.17	6	8.2	1	24
	Arc volcanoes	1.14	0.64	47	10.5	1.6	48
	Plume (hot spot) volcanoes	0.81	0.78	8	n.a.	n.a.	n.a.
	Ridge peridotite localities	0.26	0.85	29	n.a.	n.a.	n.a.
	Forearc peridotite localities	0.53	0.77	7	n.a.	n.a.	n.a.
	Arc peridotite localities	0.62	0.6	10	n.a.	n.a.	n.a.
>2,500 million years ago	Komatiite and picrite	−0.55	0.37	3	n.a.	n.a.	n.a.
	Basalt, ambient mantle	n.a.	n.a.	n.a.	8.0	0.3	21
	Basalt, arc mantle	n.a.	n.a.	n.a.	8.7	0.9	21
	Eclogite and ophiolite	n.a.	n.a.	n.a.	7.5	1.3	8

fO_2, oxygen fugacity; n.a., not applicable. V/V* represents the vanadium (V)-based fO_2 proxy, where V* is $Sc^{0.84}*Yb^{0.54}$. [a]Calculated from and refs. 197,228–230 and summarized in Supplementary Table 1. [b]log units relative to the quartz–fayalite–magnetite (QFM) buffer of ref. 45 at 1 atmosphere pressure. [c]σ represents the standard deviation.

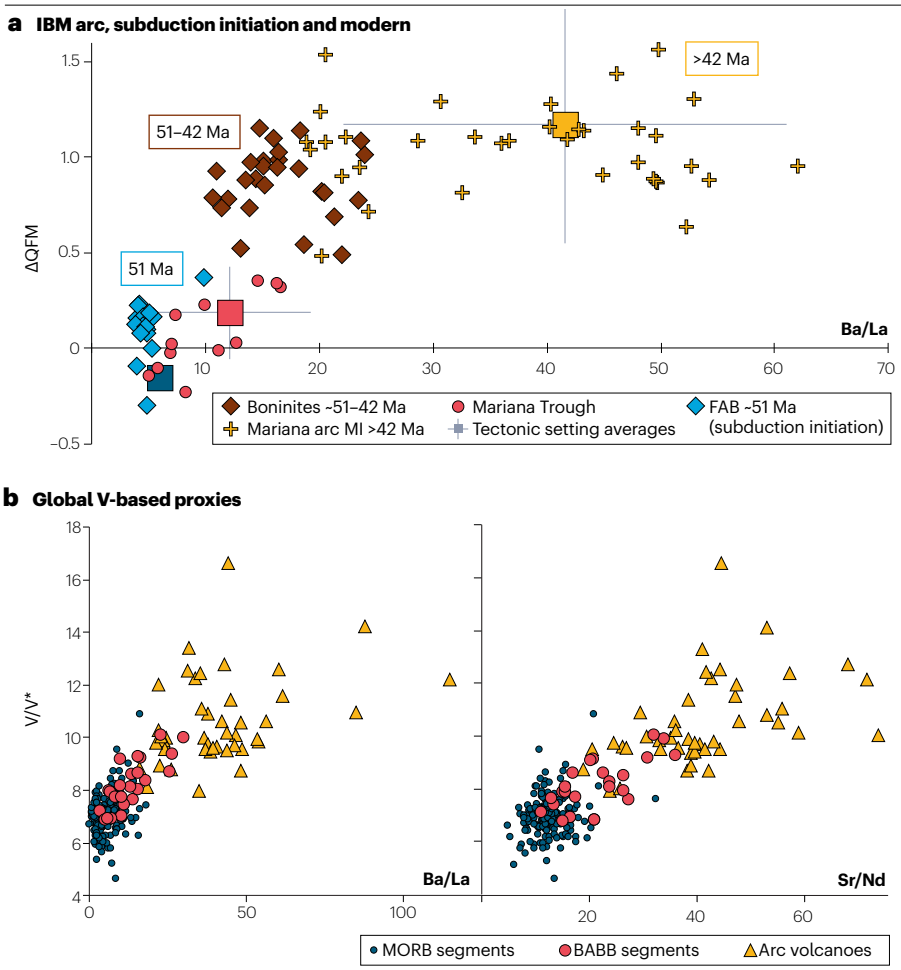

Fig. 3 | The timing and influence of subduction on fO_2. a, Thermobarometric oxygen fugacity (fO_2) and Ba/La ratios recorded by primitive (>5 wt.% MgO) and minimally degassed basalts from Izu–Bonin–Mariana (IBM). Forearc basaltic pillow lavas (FAB, blue diamond), boninitic pillow lavas (maroon diamonds), back-arc basaltic pillow lavas (Mariana Trough, pink circles), and olivine-hosted melt inclusions (MI) from Mariana arc front volcanoes (yellow cross) from subduction initiation 52 million years ago (Ma) to today's mature arc[30,32,33,76]. The large squares are average V/V* (where V* is $Sc^{0.84}*Yb^{0.54}$) and fO_2 for all samples from a tectonic setting with 1σ error bars (Table 1). **b**, Global compilation of whole rock V/V*, Ba/La and Sr/Nd for segments and volcanoes (yellow triangle), back-arc basin basalts (BABB) (pink circle) and mid-ocean ridge basalts (MORB) (dark blue circle). The data are from ref. 229. The basalts generated by decompression melting at ridges (or during subduction initiation) record melting under more reduced conditions than basalts that contain demonstrable additions from the subducting slab (for example, high Ba/La and/or Sr/Nd), suggesting that material released by the subducting slab leads to oxidized magmas in just 1–2 Myr following subduction initiation. QFM, quartz–fayalite–magnetite.

V, As, H, O and Sb, are not considered further here, because the fluxes of these elements are too small to transfer substantial redox budget.

The combined redox budgets of subducted S, C and Fe are sufficient to oxidize arc magmas[114,126–128]. S is a favoured candidate for transfer of redox budget from the slab to the mantle because S concentrations are higher in relatively undegassed, oxidized, subduction-influenced basalts compared with those from mid-ocean ridges[108]. Indeed, S concentrations are so high in these rocks that they require high fO_2 to stabilize substantial S^{6+} in the melt and thereby raise S solubility[106,108,110]. Sulfur species are also demonstrably soluble in silicate melts and aqueous fluids[129], and addition of relatively small amounts of S^{6+}-bearing fluids can increase melt fO_2 by a log unit[130].

Oxidized Fe and Mn have limited solubility in aqueous fluids at elevated temperatures[131,132]. However, these elements are more soluble in silicate-rich fluids than aqueous fluids, so a role for silicate melts, supercritical silicate-rich and possibly carbon-rich fluids is possible, though the processes are poorly understood[123,133–135].

Under subduction zone conditions, carbonate minerals dissolve to form species such as HCO_3^-, CO_3^{2-} and H_2CO_3 at concentrations up to ~1 wt.% (refs. 126,136), and CO_2 might be present as a cosolvent in H_2O–CO_2 fluids at CO_2 mole fractions of up to ~0.8 (ref. 137). However, C in the slab is modelled to be present as C^{+4} at fO_2 >~QFM − 1 under subduction zone conditions[138], so C is unlikely to be reduced and does not provide usable redox budget to common lithologies in subduction systems.

Lithologies that provide redox budget

Serpentinized mantle lithosphere has been identified as the most likely source of redox budget transferred to subarc mantle. This lithology has the highest redox budget of all the subducted lithologies[23,128,139] and shows variability in $Fe^{3+}/\Sigma Fe$ ratios that have been interpreted as a record of redox budget release[139,140].

However, thermodynamic calculations suggest that only magnetite-rich and Fe^{3+}-rich serpentinites, such as those produced at ocean–continent transitions or slow-spreading ridges, are likely to release oxidized S species during subduction. These serpentinites are represented by those found in ophiolites[141]. Magnetite and Fe^{3+}-poor serpentinites, such as the abyssal serpentinites formed at fast-spreading ridges, release reduced S instead[125,142], theoretically limiting their capacity to oxidize the mantle wedge. The Lesser Antilles Arc, which consumes crust formed at a slow-spreading ridge and where primitive arc basalts record fO_2 values as high as QFM + 4 (ref. 143), is consistent with thermodynamic model predictions. Yet the fO_2 of subarc mantle is thought to be globally elevated (Fig. 1), which is difficult to reconcile with the model results because most subduction zones on Earth today consume crust produced at relatively fast-spreading ridges.

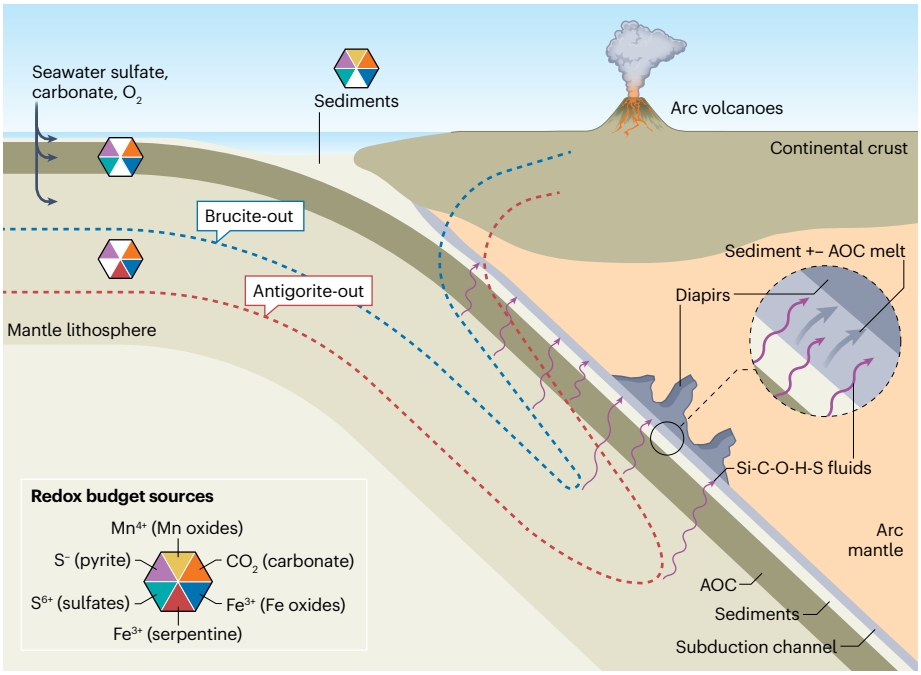

Fig. 4 | Main vectors of transport for redox budget in a subduction zone. Slab lithologies include subducted mantle lithosphere, altered oceanic crust (AOC) and sediments. Plausible candidates for transport of redox budget from slab lithologies to the overlying mantle wedge include Fe^{3+}, Mn^{4+}, S_3^-, S^{4+}, S^{6+} and C^{4+}. The redox budget could be transferred to the subarc mantle by fluids produced by brucite dehydration (brucite-out), antigorite dehydration (antigorite-out) and release of supercritical Si-C-O-H-S fluids (purple arrows), sediment ± AOC melts (grey arrows), and diapirs from the slab. The isotherms were adapted from ref. 9.

Seafloor sediments are locally rich in carbonate, oxidized Fe and Mn, and sulfate. Sediment lithologies can transfer redox budget to the wedge by melting[144], mechanical mixing[144] or reactive transport[127] and might make important contributions to the redox budget of subduction zones[107,114,123,145]. However, quantitative estimates of the redox budget of locality-specific arc inputs and outputs are rare[114] and slab-interface lithologies record complex and highly heterogeneous redox conditions ranging from QFM − 1 to QFM + 12 (refs. 146–150). Complex interactions between lithologies within the slab interface might facilitate release of redox budget[125,127,151] (Fig. 4).

The Ca/(Ca + Mg + Fe) content of sediments and the thermal structure of the subduction zone are first-order controls on the release of sulphate and a characteristic suite of sulfur-associated elements (for example, Cu, As, Zn and Pb) that can be recognized in individual arcs[107]. The S concentration of sediment melts formed in the presence of anhydrite is higher than those formed in the presence of pyrrhotite, which implies that oxidized systems have an enhanced capacity to mobilize redox budget[152], which is consistent with measured basalt S characteristics[108]. However, slab-derived Si-rich melts formed in the presence of anhydrite might carry insufficient S^{6+} to explain the abundance of S in the subarc mantle without a contribution from additional mechanisms[153].

Subducted mafic rocks can also provide redox budget. Inclusions within garnet in eclogite from Sifnos, Greece, record a shift towards more reducing conditions during metamorphism, attributed to release of oxidized sulfate-bearing fluids during lawsonite breakdown[154,155]. Slab melts of altered oceanic crust fluxed by serpentinite-derived aqueous fluids are another promising vector for transfer of slab-derived sulfate[80].

The mechanisms that link subduction to the redox budget of the mantle wedge must be consistent with the observed production and oxidation of subarc mantle within 1–2 Myr of subduction initiation[32,33]. The heterogeneity in oxidation state (as documented in ref. 85) and typical mantle flow rates of tens of kilometres per million year require dominantly vertical, rather than horizontal, transfer of slab-derived material, if slab-derived material is to reach the arc-magma source zone.

A range of mechanisms, including diapirism[144,156,157], a metasedimentary redox filter[127], and slab relamination[158,159] might provide suitably rapid transfer mechanisms (Fig. 4). Alternatively, seismicity in some slabs is associated with fluid production, including carbonatitic melts at 500–700 km depth[160]. Seismicity might help to drive migration of silica-rich fluids that can carry a substantial cargo of Fe^{3+}, but seismicity-related fluid transfer has only been recognized at shallower depths of less than ~300 km (ref. 161).

All models that invoke transfer of redox budget to effect change in magmatic fO_2 should be evaluated with caution. The results of thermodynamic models are limited by poorly known thermodynamic data, equations of state and activity–composition relationships for the S-bearing, C-bearing and Fe-bearing species found at high pressures in subduction zones. In addition, internal rock buffers are not always parallel to the QFM buffer commonly used as a reference for calculated changes in melt redox state (Box 1). More importantly, even substantial transfers of redox budget might not perturb the fO_2 of a strongly buffered system (Box 1). For all of these reasons, conclusions based solely on model results are less robust than those backed by observations.

Archaean to present-day mantle fO_2

Models for mantle fO_2 evolution over Earth's history have undergone major revisions since the turn of the millennium and remain hotly debated. This section provides an overview of evidence from the rock record for the evolution of mantle fO_2 during the Archaean.

Possible links to the GOE

Atmospheric oxygen originated near 2.35 Ga (the GOE) from oxygen-producing photosynthesis[162], but the solid Earth's role might

have been to titrate, buffer, delay or hasten, atmospheric and oceanic oxygenation via a myriad of mechanisms[163,164]. Early models for mantle fO_2 following Earth's global magma ocean phase presumed a reduced mantle during the Hadean, due to its equilibrium with the early formed metallic core[12]. Volcanism from the Archaean mantle was believed to have released reduced gas species that were a sink for surface O_2. Over time, the mantle might have oxidized as an outcome of ongoing subduction[165], with mantle-derived gases becoming less reducing and allowing accumulation of O_2 in the atmosphere and ocean.

Evidence from V partitioning between olivines and melts in Archaean komatiites[20] challenged the assumption of a reduced Archaean mantle, instead suggesting that the earliest rocks record mantle fO_2 similar to the present day. Additional evidence from Archaean basalts[35,36] and Hadean zircons[37] also supported an oxidized Archaean mantle. Moreover, mantle mixing calculations indicated that oxidation of the entire mantle via subduction would be difficult to achieve on the likely timescales[23]. This evidence makes a causal link between oxidation of the mantle and the GOE unlikely.

V concentrations in Archaean komatiite olivines[41], and V/Sc of Archaean metabasalts[40] have renewed debate on a potential causal link between mantle fO_2 and the GOE by suggesting a large increase in the fO_2 and (or) the Fe^{3+} budget of the mantle during the Archaean. Other alternative models also emerged that link the GOE to mantle redox via indirect means, such as through changes in magmatic temperature[166,167], degassing pressure[168,169] (though see[79]) or mantle potential temperature and depth of melting[58,71,130]. Therefore, support for a causal link between mantle fO_2 and the GOE has varied and it is timely to review evidence from the rock record.

Spinel Fe^{3+} and Cr–V systematics

The abundance of multivalent elements, such as Cr and V, in spinel-saturated, mafic magmas is strongly controlled by fO_2 (ref. 170). The covariation of Cr, V and Mg in mafic volcanic rocks from the Archaean is similar to those from the present day, requiring they formed at similar fO_2 (ref. 36). The chemistry of Cr-rich spinels in mafic mantle-derived volcanic rocks or preserved as detritus in sedimentary rocks would vary with time if mantle fO_2 varied, but this is not observed[36,171].

Komatiite lava

An unchanged mantle fO_2 since the Archaean has been challenged based on fO_2 estimates using V olivine–liquid partitioning ($D_V^{ol/liq}$). Except for one 3,550 million years ago (Ma) datum, $D_V^{ol/liq}$ from individual komatiite and picrite lava flows have been used to suggest a steadily increasing mantle fO_2 over time[41,172]. However, similar data from basalts formed over present-day ridges[173] and plumes[174], collected and interpreted using identical techniques, span the entire range of fO_2 as the Archaean komatiites and picrites (Fig. 5a). Moreover, fO_2 estimated from $D_V^{ol/liq}$ measured in present-day MORB[173] encompass and exceed, by more than a factor of 2, the narrow range of fO_2 estimated oxybarometrically from MORB $Fe^{3+}/\Sigma Fe$ (refs. 46–48). The rock record of $D_V^{ol/liq}$ might simply reflect the same heterogeneity in mantle fO_2 over time as is observed in the present day, rather than any steady temporal evolution.

$D_V^{ol/liq}$ preserved in Archaean komatiite flows contrasts with evidence from olivine-hosted melt inclusions, even from the same lava sequence[175–178]. This observation also suggests heterogeneity in fO_2, rather than any systematic temporal variation. The $D_V^{ol/liq}$ of the melt inclusions show the fO_2 of komatiite was similar to MORB[179] (Fig. 5a and Table 1). The melt inclusions can be chemically compromised[180] by reequilibration, but this effect does not change fO_2 estimates from $D_V^{ol/liq}$ (ref. 181).

The komatiite/picrite dataset ($N = 15$) for $D_V^{ol/liq}$ is far smaller than the dataset based on V concentration systematics applied to several hundred basalt[35] or peridotite samples over time[182]. Further, komatiite is a minor component (<10%) of volcanic stratigraphies[183] and probably represents plume mantle, not the greater ambient convecting mantle[184]. Using only komatiites as a probe of temporal change in mantle fO_2 represents a sampling bias to a melt that is unrepresentative of average mantle over most of the geologic record, which is better recorded by basalts[35].

A further complication is that higher temperature melts generated in the garnet field, such as komatiites, might have equilibrated at lower[71,130] or higher[58] fO_2 at the same bulk mantle $Fe^{3+}/\Sigma Fe$ as melts generated in the spinel field, depending on the depth of melting (Box 2). Although great debate exists about the tectonic conditions required to extract and erupt such deep-seated melts, there is agreement that komatiite lavas and residues could record lower fO_2 than Archaean (or present-day) basalts and residues, even if derived from mantle peridotite with the same $Fe^{3+}/\Sigma Fe$ (refs. 58,71).

Eclogite xenoliths and massifs

To obviate the bias introduced by sampling komatiites, eclogite xenoliths and ophiolite massifs have been used to sample the convecting mantle to study its fO_2 over time. Precambrian (4,600–541 Ma) eclogite xenoliths and ophiolite massifs have been interpreted as remnants of ancient basalt derived from the convecting mantle – comparable with present-day MORB. These samples were either exhumed as massifs or subducted and later incorporated into the mantle lithosphere where they were sampled as xenoliths by kimberlite[185,186]. The age of eclogite xenoliths in the mantle can be estimated using Re–Os systematics[40]. These rocks document a protracted metasomatic history encompassing a billion years of storage in the lithosphere[187–190].

Caveats exist for the use of eclogite xenoliths or massifs as records of ambient mantle fO_2. There are far fewer eclogite xenoliths or massifs that can be selected to reconstruct Archaean basalts than surface basaltic lavas (now greenstone). Many eclogite bulk compositions are atypical of compositions produced by mantle melting; they might not be representative of basalt at all but, rather, melt-rock reaction or residues of melting[191,192]. For the Precambrian ophiolite massifs[40], as is the case for their Phanerozoic (<541 Ma) analogues, such rocks most likely formed in the suprasubduction environment – having more to do with the subduction than ridge spreading and the convecting mantle.

Regardless of such caveats, these rocks have been used to infer changes in mantle fO_2 over time. After geochemical filtering for the identification of MORB-like chemical traits and removing the effects of metasomatism and differentiation, the V/Sc ratios in eight xenolith, ophiolite and massif localities have been used to infer a temporal trend in fO_2 and a more reduced Archaean mantle[40,193,194]. However, using identical dataset and filters[193] (Supplementary Note 3), V/V* (Fig. 5 and Supplementary Fig. 4), V/Sc and V/Ti (Supplementary Fig. 5) show an overlap with modern MORB with little-to-no temporal trend (Fig. 2a and Fig. 5d).

Basalts over time

The V/V* proxy can be applied to query temporal variation in mantle fO_2 using ancient mantle-derived basalts. Although their exact tectonic provenance is less certain, such basalts are the least biased, best preserved and most abundant mantle-derived rock in the geologic record[6,195,196].

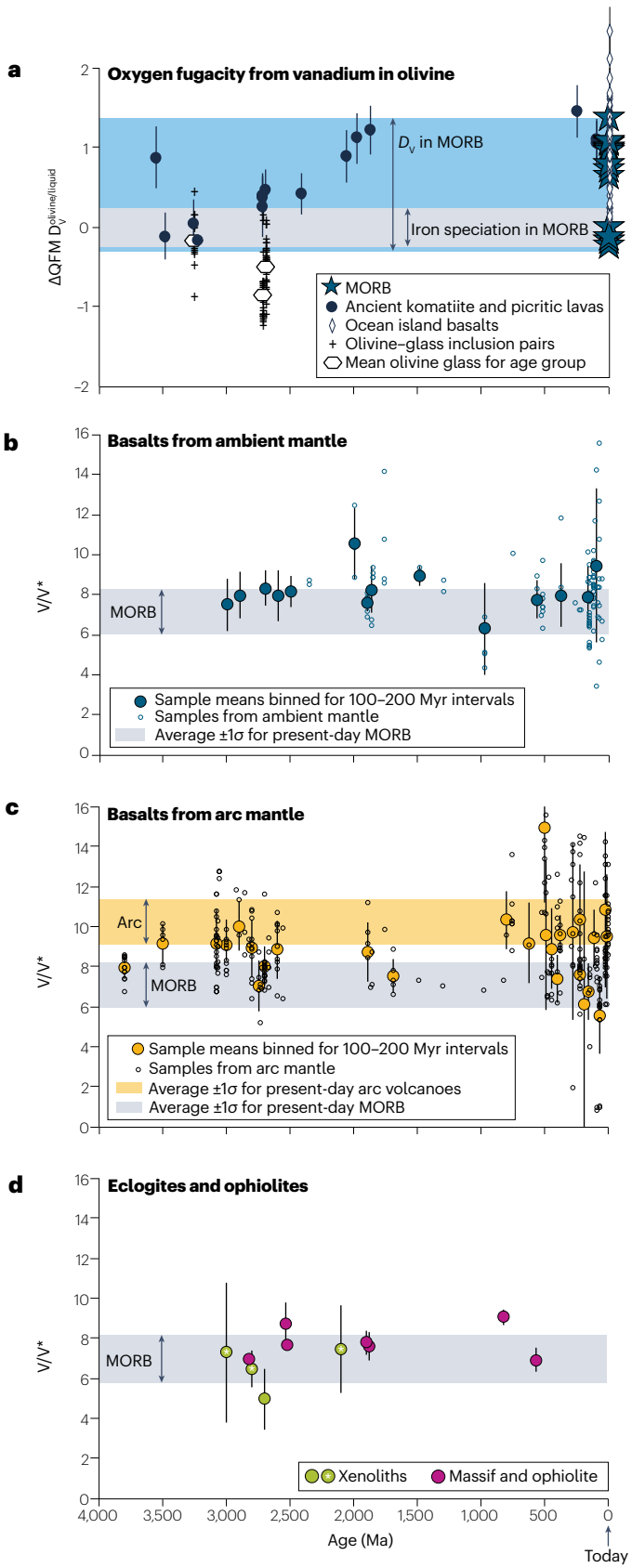

Fig. 5 | fO_2 (calculated from modelled $D_V^{ol/liq}$) and V/V* from Archean and present-day rocks. a, Estimates of oxygen fugacity (fO_2) (as published, without modification) for present-day mid-ocean ridge basalts (MORB) lavas (blue stars and light blue band)[173], present-day ocean island basalts[174] (open narrow diamonds) and ancient komatiite and picritic lavas[41,172,244] (filled black circles), all modelled from the V-in-olivine approach of ref. 174. Measured $D_V^{ol/liq}$ between olivine and glass inclusion pairs in komatiites (crosses) with the mean for each age group (white hexagons)[176–178]. The grey band indicates the fO_2 inferred from iron speciation in present-day MORB[46,48]. **b**, The V/V* (where V* is $Sc^{0.84}*Yb^{0.54}$) proxy for basaltic lavas over time from ambient mantle sources[71] using data from ref. 196 for samples <2,500 million years ago (Ma) and ref. 197 for samples >2,500 Ma, filtered using criteria from refs. 71,197. The large filled circles are sample means binned for time intervals (100–200 Myr). **c**, The V/V* proxy for basaltic lavas over time from arc mantle sources[71] using data from refs. 6,196 for samples <2,500 Ma and ref. 197 for samples >2,500 Ma filtered using criteria from refs. 71,197. The large filled circles are means for binned time intervals (100–200 Myr). **d**, The V/V* proxy for bulk analyses of metabasalts (eclogite xenoliths, ophiolites and orogenic eclogite massifs) from ref. 40 calculated with data from refs. 40,187–189,193,245–248 and filtered with criteria from ref. 40. Three eclogite xenolith localities (green circle with asterisk) from ref. 40 have MgO >12 wt.% so do not meet the V/V* filtering criteria (or V/Sc filtering criteria). The inclusion or exclusion of these samples does not impact our conclusions. The MORB (grey) and Arc (yellow) bands are V/V* averages measured at present-day ridges and arcs, ±1σ (Table 1 and ref. 229). The bulk analyses in panels **b**–**d** are compiled from ref. 230. A second version of this figure is provided with alternative filters applied (Supplementary Fig. 4), as well as V/Ti and V/Sc as a function of time (Supplementary Fig. 5) for the same samples and localities. There is no statistically significant temporal trend in fO_2 in mantle-derived rocks since the Archaean using any vanadium-based redox proxy.

V/V* for ancient basalts are calculated with a conservative filter of 6 < MgO wt.% < 12 (before magnetite-in) and Dy/Yb <1.8, to eliminate samples with garnet influence[100]. Previously published and stringently filtered compilation datasets are used for samples younger than 2.5 Ga (refs. 6,196) and older than 2.5 Ga (ref. 197). Those datasets filtered the samples to have loss on ignition <6 wt% and CaO >13.81 − 0.274*MgO − a criterion for magmas from peridotite-only sources[198]. Basalts from non-arc (or ambient) convecting mantle were distinguished from arc basalts using a threshold of primitive-mantle-normalized Nb/La >0.75 (refs. 71,197 and see Supplementary Note 3 for details).

There are no statistically significant differences in the average V/V* between any of the groups (ambient versus arc (Table 1)). The resulting V/V* of all ancient basalts and the fO_2 show no systematic change over 3.5 Gyr — across any time boundary or environmental events including the GOE (Fig. 5b,c).

A caveat in global analyses of basalts is that the record older than 200 Ma is biased to magma erupted and preserved on continents, rather than in the oceanic realm. However, even if the assumption that eclogite xenoliths represent subducted ocean crust older than 2 Ga (refs. 185,186) is adopted, they do not notably differ from modern terrestrial basalts and show no trend in V/V* and mantle fO_2 with time (Fig. 5d).

This reassessment shows the previous use of V/Sc as a redox proxy in basalt[73], eclogite or metabasalt[35,40,193] might be affected by crystal fractionation (Fig. 2a and Supplementary Fig. 1). Application of the V/V* proxy, which is unaffected by crystal fractionation, to magmas derived from garnet-free mantle, captures the breadth of mantle-derived mafic and ultramafic magmatism over 3.5 Gyr. The V/V* proxy shows a lack of systematic change in fO_2 with time in the convecting ambient upper mantle. This result is not an effect of temperature because our analysis

of experimental data shows $D_V^{olivine/melt}/D_{V^*}^{olivine/melt}$ ($D_{V/V^*}^{ol/melt}$) and $D_V^{cpx/melt}/D_{V^*}^{cpx/melt}$ have no significant temperature dependence (Fig. 2d and Supplementary Fig. 2). The invariance of V/V* also parallels the lack of profound changes in basalt compositions that can be assigned to any major singularity in earth evolution, such as the GOE or the advent of subduction[199]. This invariance raises a central question for Earth evolution. The question of how the oxygen balance in the deep Earth deviated from that of an early Hadean magma ocean in equilibrium metallic core remains. Exploration and testing of plausible magma ocean models are required to address this question.

Hadean mantle fO_2

In <100 Myr, metal core segregation from the Hadean magma ocean was nearly complete[200], leaving a system in which silicate melt, silicate minerals, core-forming metal and Earth's first atmosphere strove to equilibrate over an enormous range of pressures and temperatures. At constant oxygen content, a planetary mantle will span a range of fO_2 values as gradients in pressure impose changes to the composition of solid and liquid phases. Because complex fO_2-dependent coevolution of magma oceans and atmospheres has a defining role in planetary habitability[14,201], research interest in planetary magma oceans is high, and the field is rapidly evolving. This section discusses the constraints and models that dominate conversation about Hadean mantle fO_2.

Constraints on magma ocean fO_2

The compositions of meteorites (Earth's putative building blocks) and the composition of Earth's mantle, atmosphere and crust place observational constraints on the fO_2 of Earth's Hadean mantle. The rock record is sparse and model uncertainty is high.

Segregation of molten iron metal from silicate melt at low pressure during Earth's magma ocean stage would have imposed an fO_2 well below iron–wüstite (IW, Fe–FeO) equilibria (Box 1). The concentrations of FeO and siderophile (iron-loving) elements (for example, Ni, Co and W) in Earth's present-day mantle constrain the average polybaric fO_2 of the magma ocean to ~IW − 2 (refs. 12,13,202,203).

The mass and composition of the first atmosphere was determined by Earth's massive magma ocean[15,204] (Supplementary Fig. 7). Yet, degassing reactions at high temperature and low fO_2 remain ill-constrained and the interplay between shallow and deep redox reactions that would have governed surficial magma ocean degassing remains elusive. Thermodynamic calculations give a lower bound of IW − 3 imposed by a magma ocean saturated in graphite in equilibrium with a dense CO-dominated atmosphere. An upper bound of IW + 3 is imposed by sulfide saturation in equilibrium with atmospheric SO_2 (ref. 15). The chondritic deuterium/hydrogen ratio of Earth's oceans further limits the amount of H_2 that could have been lost from Earth's earliest atmosphere to space, implying that the late-stage, shallow magma ocean must have equilibrated at fO_2 > IW + 1 (ref. 205).

Post-dating the magma ocean stage, only a handful of zircon crystals survive to represent the Hadean terrestrial rock record. These zircons record crustal fO_2 values similar to those of present-day granitic zircons (scattered around QFM) – orders of magnitude above that recorded by zircons from the lunar magma ocean[37,206] (scattered around IW).

Based on current observational constraints, the range of possible fO_2 in the upper mantle at the end of the terrestrial magma ocean phase spans more than five orders of magnitude ($-2 \lesssim IW \lesssim +3$). The preponderance of evidence points to a shallow magma ocean that was similar to or more oxidized than the IW buffer by the end of the Hadean. A myriad of models, discussed below, plausibly explain the rapid oxidation of Earth's mantle during the Hadean to reach the fO_2 conditions recorded by Hadean zircons and Archaean rocks.

Open-system processes

Open-system processes offer plausible, albeit ad hoc, pathways for changing magma ocean fO_2 during and just after Earth's accretion from planetary embryos (Fig. 6). Progressively more oxidizing accretionary inputs from space, so-called heterogeneous accretion[207–209], provide one oxidation mechanism. Reduced outputs to space, for example, H_2 loss[165,210–212], provide another oxidation mechanism, albeit one that might be limited[205]. Perhaps counterintuitively, accretion from planetary embryos with H_2-rich atmospheres might also be consistent with mantle oxidation[213], as discussed below. Because open-system processes are difficult to quantify or test, only closed-system oxidation mechanisms are discussed below in detail.

Magma ocean oxidation mechanisms

A large-radius planet (for example, greater than or equal to Earth's radius) makes possible a range of magma ocean oxidation mechanisms owing to higher pressures and temperatures of equilibration (for example, in comparison with Mars, which is smaller and has a more reduced mantle[44]) (Fig. 6).

A gaseous atmosphere, a silicate mantle and an iron-alloy core are key reservoirs that must be considered in any successful model of Hadean redox. Due to their massive redox budgets, equilibrium between the mantle-forming silicate liquid and core-forming metal alloy established an initial fO_2 and $Fe^{3+}/\sum Fe$ of the liquid at depth. The fO_2 of the shallow magma ocean then dictates volatile speciation in the overlying atmosphere (Fig. 6). Equilibration of silicate melt and liquid metal alloy at low pressure establishes very low fO_2 and, hence, a reduced atmosphere[12]. But the high pressure of metal–silicate equilibrium in a terrestrial magma ocean requires consideration of the relationship between the $Fe^{3+}/\sum Fe$ of silicates and fO_2 at higher pressures. Three possible mechanisms are reviewed (Fig. 6).

In the first possible mechanism, silicon dissolution into core alloy at high pressure (SiO_2 (mantle melt) + Fe (core alloy) → FeO (mantle melt) + Si (core alloy)), might have worked to increase mantle FeO concentration, and hence fO_2, as the planet grew[202,214]. This mechanism is facilitated by high pressures and temperatures and low fO_2 (the latter potentially facilitated by H dissolution into the magma ocean and, ultimately, the metal core from a primordial atmosphere[213]). By contrast, other ultrahigh-pressure experiments challenge this view, suggesting that oxygen dissolution in the metal core could have resulted in a magma ocean that evolved from relatively oxidizing to relatively reducing[215].

The second possible mechanism stems from experiments that show the presence of abundant Fe^{3+} in minerals in equilibrium with metal and under the low fO_2 (<IW − 2) conditions of core formation. Lower mantle pressures (>24 GPa) facilitate disproportionation of magmatic $Fe^{2+}O$ and stabilize Fe^{3+}-rich perovskite (Fe^{3+}–pv) and Fe^0–metal (ref. 38). If the Fe^0–metal sank to the core and left Fe^{3+}-rich perovskite in the mantle, this would cause net oxidation of the lower mantle[13,38,216]. Mantle overturn or convection would then cause an oxygen gain (an increase in redox budget) in the upper mantle – an oxygen pump[13] (Fig. 6).

The third mechanism relies on the observation that the $Fe^{3+}/\sum Fe$ ratio of a silicate liquid in fO_2 equilibrium with metal at high pressure is

not the same as at low pressure (Box 2). At shallow upper mantle pressures (≲10GPa), the fO_2 of liquid silicate at constant $Fe^{3+}/\sum Fe$ increases with pressure[217,218] (or $Fe^{3+}/\sum Fe$ decreases with pressure at constant relative fO_2). However, experimental observations[219–221] and molecular dynamic calculations[222] suggest that this trend reverses at yet higher pressures. A reversal might enable $Fe^{3+}/\Sigma Fe$ ratios in excess of 0.03 (similar to the ratio of 0.036–0.037 estimated for the present-day upper mantle[54]) to be stable at the high inferred magma ocean pressures of metal–silicate equilibrium[220] (28–53 GPa) (ref. 223). If such high $Fe^{3+}/\Sigma Fe$ ratios could persist to the surface via vigorous, isochemical convection, it would enforce high fO_2 at the low-pressure magma ocean–atmosphere interface. Metal–silicate equilibrium at depth therefore need not preclude an oxidized H_2O–CO_2 atmosphere[16] (Fig. 6).

If the present-day $Fe^{3+}/\Sigma Fe$ ratio of the upper mantle corresponds to that of the magma ocean, 1-atm high-temperature data on peridotitic liquids suggest that the Earth's magma ocean fO_2 was from ~IW − 0.4 to IW + 2 at the surface just prior to crystallization, stabilizing a CO–CO_2 dominated atmosphere[220,223,224].

Magma ocean redox budgets

Relating observations of rocks and minerals to the intrinsic property of fO_2 is essential for comparison to experiments and thermodynamic models but does not predict the consequences for mass transfer of oxidants or reductants or charge-transfer reactions as conveniently as redox budget (Box 1). Redox exchange between Fe^{3+} and Cr^{2+} during magma ocean cooling provides one example whereby Cr^{2+} might have consumed Fe^{3+} (in other words, reduced Fe^{3+}), implying that either the magma ocean was yet more oxidized or that other processes, such as the oxygen pump and open-system processes, boosted Fe^{3+} in the silicate melt to compensate the estimated 0.35 wt.% Fe_2O_3 consumed by Cr^{2+} oxidation[223]. Similar consideration of S, C, H and Fe via closed and open-system processes and the linkage between fluxes and thermodynamics is necessary, but these considerations remain nascent[225], lacking observational constraints. The planetary science community is working intensively to develop numerical codes that connect magma ocean processes to the growth of primordial outgassed atmospheres[226,227], in the hope that these codes will be applicable to exoplanets similar to the Hadean Earth. The debate on the fO_2 of the magma ocean therefore continues and provides an area ripe for future research.

Summary and future perspectives

There is widespread agreement that basalts sampled at mid-ocean ridges record fO_2 near the QFM buffer. To constrain the depth and mechanism of mantle melting and its relationship to geophysical observables, progress is needed to experimentally quantify the coevolution of fO_2 and the $Fe^{3+}/\Sigma Fe$ ratios in melts and minerals above and below

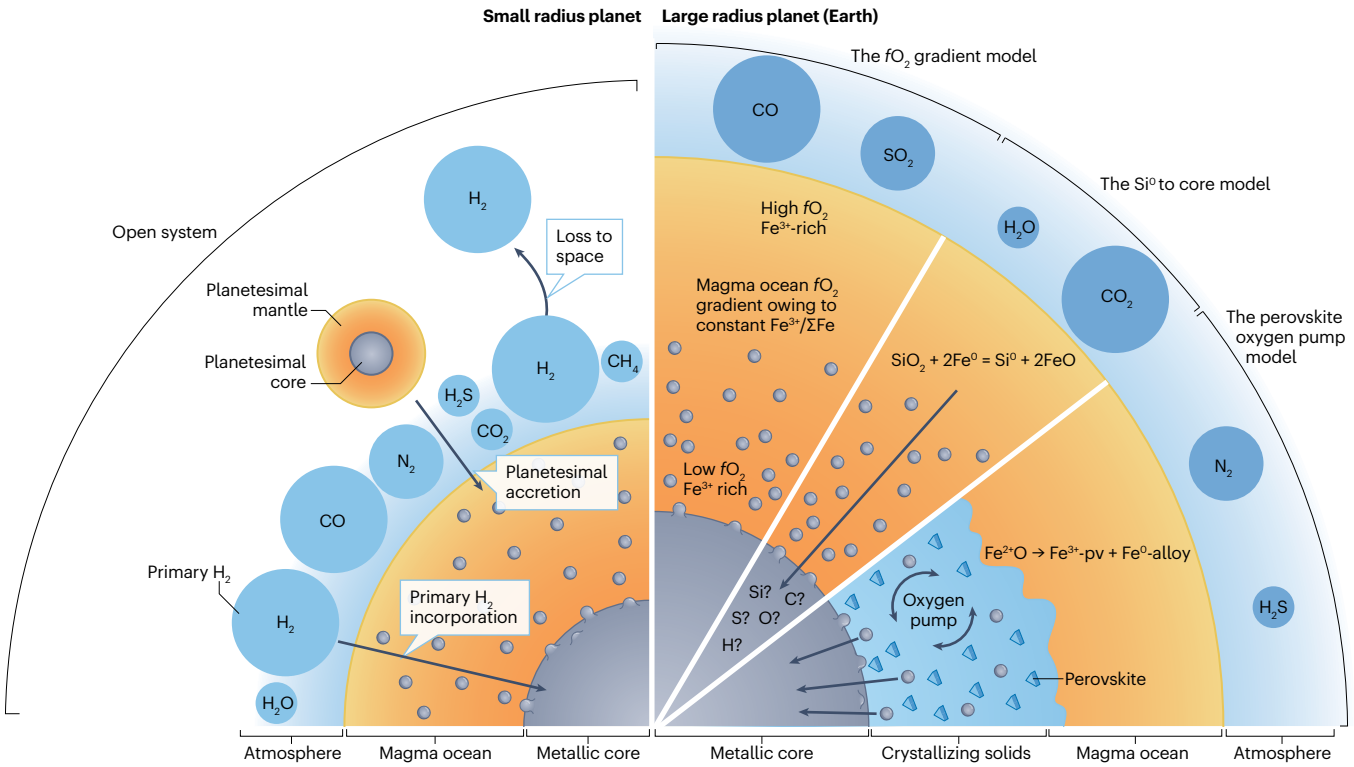

Fig. 6 | Mechanisms to oxidize a Hadean magma ocean. A schematic cross section through a small radius planetesimal (left) and a larger radius planet (-Earth) (right) and their atmospheres, illustrating possible pathways to an oxidized shallow magma ocean and atmosphere system. Left: open-system mechanisms that could plausibly operate on planets smaller than Earth, such as the addition of progressively more oxidizing accretionary material, loss of H_2 to space and primary H_2 incorporation. Right: mechanisms that require high, Earth-like, pressures, including increased stability of $Fe^{3+}/\Sigma Fe$ (but low fO_2) in silicate liquid, partitioning of Si^0 into the core and disproportionation of $Fe^{2+}O$ to generate Fe^{3+}-rich perovskite that remains in the mantle and Fe^0-rich metal alloy that sinks to the core. Although the atmosphere of the small planetesimal is dominated by reduced volatile species, that of the larger planet is dominated by oxidized species (volatile abundance schematically represented by size of the volatile 'sphere' in the atmosphere).

Glossary

Activity–composition relationships
The relationship between a chemical component's concentration and its chemical activity, or so-called effective concentration.

$D_V^{ol/liq}$
The olivine–liquid (olivine–silicate melt) partition coefficient for vanadium. When the melt is not present, its V concentration must be estimated from a model.

Great Oxidation Event
(GOE). A permanent rise in atmospheric oxygen between 2.4 and 2.1 billion years ago.

Incompatible element
An element that prefers to concentrate in the silicate liquid compared with a coexisting mineral, or minerals, at equilibrium.

Magma ocean
A planet's partially or completely molten proto-mantle, owing to additional energy sources during planetary accretion and core formation (Earth's occurred in the first ~100 Myr).

Oxygen fugacity (fO_2)
An intensive thermodynamic variable that quantifies the chemical activity of oxygen in a system.

Partition coefficient
($D_{\text{element } i}^{\text{solid/liquid}} = \frac{\text{concentration } i \text{ in solid}}{\text{concentration } i \text{ in liquid}}$).
A quantification of how an element is distributed between mineral, melt and metal phases at equilibrium and is <1 for an incompatible element and >1 for a compatible element.

Redox
Short for oxidation–reduction reaction in which the reactants change oxidation state. Used informally (and potentially with purposeful ambiguity) to mean both oxidation state and (or) fO_2.

Redox budget
Extensive variables are used to measure the capacity or transfer of oxidizing or reducing agents.

the solidus. Few existing experiments at known fO_2 have characterized $Fe^{3+}/\Sigma Fe$ of coexisting phases, and more are needed. Theoreticians must then incorporate such experimental constraints to improve computational thermodynamic models.

Lavas in proximity to subduction zones record fO_2 values that are higher on average than those at ridges, and multiple lines of evidence, including a new V/V* proxy, support a mantle origin for the oxidized signature. Determining how convergent margins oxidize the mantle wedge requires further work. Sediments, mafic ocean crust and mantle lithosphere all have the potential to provide redox budget to the zone of arc melt production via a transport agent that has yet to be conclusively identified; however, S is a strong candidate. Further experimental and observational work are needed to better constrain the mass transfer mechanisms and when in Earth's history arc mantle became oxidized.

Redox-sensitive trace elements such as V quantify relative fO_2 in basalt sourced from spinel-peridotite — even if the absolute fO_2 is model-dependent. The fO_2 recorded by Archaean komatiites span the same range as modern plume-derived and ridge-derived basalts using the same $D_V^{ol/liq}$ technique and imply no temporal trend. The fO_2 implied by the V/V* of hundreds of ancient basalts sourced from the depleted mantle do not show any statistically significant temporal trend in fO_2 either. Thus, there is no clear evidence for a change in mantle oxidation state since the Archaean. That said, mantle-derived melts older than 200 Ma in the geologic record are preserved only in the continental realm — as lavas in Archaean greenstone belts, as flood basalts or as arcs built on continental crust — which makes comparisons with the modern Earth indirect. A comparison could be facilitated by further developing redox proxies, such as V/V*, so that they can be applied to melts from garnet-bearing mantle sources.

Oxidation processes during the Hadean are of great importance for the evolution of the early Earth. Plausible closed-system processes for oxidation on an Earth-sized planet include exchange of Si, O, C, H, S, P and Fe between the core and mantle, disproportionation of FeO followed by Fe^0 loss to the core and Fe^{3+}-perovskite gain in the mantle, and equilibration of alloy and melt at high pressure that stabilizes a liquid at low pressure with high $Fe^{3+}/\Sigma Fe$ ratio. Capturing redox dynamics in convective and reactive magma oceans requires new coupled geodynamic and thermodynamic models linking planetary interiors to surfaces during the magma ocean stage. Such models must also accommodate irreversible escape processes, including redox-sensitive light element incorporation in the core and outgassing to space, while abiding by timing, thermodynamic and mass-balance (redox budget) constraints. Experimental constraints on the behaviour of redox-sensitive elements under these extreme pressure–temperature–fO_2 conditions and their incorporation into thermodynamic models is an important next step for the community to understand the earliest events that shaped planet Earth.

Data availability

The oxybarometic data can be found in ref. 228 and https://doi.org/10.60520/IEDA/113694. Geochemical data can be found in ref. 229 and https://doi.org/10.60520/IEDA/113251. The vanadium redox proxies applied to mantle-derived magmas over time can be found in ref. 230 and https://doi.org/10.26022/IEDA/112512.

Published online: 4 November 2025

References

1. Stagno, V., Ojwang, D. O., McCammon, C. A. & Frost, D. J. The oxidation state of the mantle and the extraction of carbon from Earth's interior. *Nature* **493**, 84–88 (2013).
This paper shows how the redox-depth profile of the upper mantle and $Fe^{3+}/\Sigma Fe$ control the depth of carbonate-fluxed redox melting.
2. Stagno, V. & Frost, D. J. Carbon speciation in the asthenosphere: experimental measurements of the redox conditions at which carbonate-bearing melts coexist with graphite or diamond in peridotite assemblages. *Earth Planet. Sci. Lett.* **300**, 72–84 (2010).
3. Dasgupta, R. et al. Carbon-dioxide-rich silicate melt in the Earth's upper mantle. *Nature* **493**, 211–215 (2013).
4. Osborn, E. F. Role of oxygen pressure in the crystallization and differentiation of basaltic magma. *Am. J. Sci.* **257**, 609–647 (1959).
5. Bucholz, C. E., Stolper, E. M., Eiler, J. M. & Breaks, F. W. A comparison of oxygen fugacities of strongly peraluminous granites across the archean–proterozoic boundary. *J. Petrol.* **59**, 2123–2156 (2018).
6. Stolper, D. A. & Bucholz, C. E. Neoproterozoic to early phanerozoic rise in island arc redox state due to deep ocean oxygenation and increased marine sulfate levels. *Proc. Natl Acad. Sci. USA* **116**, 8746–8755 (2019).
7. Holloway, J. R. & Blank, J. G. Application of experimental results to C–O–H species in natural melts. *Volatiles Magmas* **30**, 187–230 (1994).
8. Mungall, J. E. Roasting the mantle: slab melting and the genesis of major Au and Au-rich Cu deposits. *Geology* **30**, 915–918 (2002).
9. Richards, J. P. Magmatic to hydrothermal metal fluxes in convergent and collided margins. *Ore Geol. Rev.* **40**, 1–26 (2011).
10. Sillitoe, R. H. Porphyry copper systems. *Economic Geol.* **105**, 3–41 (2010).
11. Luth, R. W. & Stachel, T. The buffering capacity of lithospheric mantle: implications for diamond formation. *Contrib. Mineral. Petrol.* https://doi.org/10.1007/s00410-014-1083-6 (2014).
12. Walter, M. J., Newsom, H. E., Ertel, W. & Holzheid, A. in *Origin of the Earth and Moon* (eds Canup, R. M. & Righter, K.) 265–290 (Univ. Arizona Press, 2000).
13. Wade, J. & Wood, B. J. Core formation and the oxidation state of the Earth. *Earth Planet. Sci. Lett.* **236**, 78–95 (2005).

14. Zahnle, K., Schaefer, L. & Fegley, B. Earth's earliest atmospheres. *Cold Spring Harb. Perspect. Biol.* **2**, a004895 (2010).
15. Gaillard, F. et al. Redox controls during magma ocean degassing. *Earth Planet. Sci. Lett.* https://doi.org/10.1016/j.epsl.2021.117255 (2022).
16. Hirschmann, M. M. Magma ocean influence on early atmosphere mass and composition. *Earth Planet. Sci. Lett.* **341-344**, 48–57 (2012).
This paper relates magma ocean depth, $Fe^{3+}/\Sigma Fe$, fO_2, and atmospheric composition, and suggests that core-forming alloy in equilibrium with liquid silicate at high pressure and low fO_2 could be consistent with a relatively oxidized primordial atmosphere.
17. Wood, B. J. & Virgo, D. Upper mantle oxidation state — ferric iron contents of lherzoline spinels by Fe-57 Mossbauer spectroscopy and resultant oxygen fugacities. *Geochim. Cosmochim. Acta.* **53**, 1277–1291 (1989).
18. Ballhaus, C., Berry, R. F. & Green, D. H. High-pressure experimental calibration of the olivine-ortho-pyroxene-spinel oxygen geobarometer — implications for the oxidation-state of the upper mantle. *Contrib. Mineral. Petrol.* **107**, 27–40 (1991).
19. Kress, V. C. & Carmichael, I. S. E. The compressibility of silicate liquids containing Fe_2O_3 and the effect of composition, temperature, oxygen fugacity and pressure on their redox states. *Contrib. Mineral. Petrol.* **108**, 82–92 (1991).
20. Canil, D. Vanadium partitioning and the oxidation state of Archaean komatiite magmas. *Nature* **389**, 842–845 (1997).
This paper experimentally calibrates $D_V^{(ol/liq)}$ and applies it to Archean komatiites, challenging the then-dominant paradigm that the Archean mantle was more reducing than the modern mantle.
21. Buddington, A. & Lindsley, D. Iron–titanium oxide minerals and synthetic equivalents. *J. Petrol.* **5**, 310–357 (1964).
22. Evans, K. A. Redox decoupling and redox budgets: conceptual tools for the study of earth systems. *Geology* https://doi.org/10.1130/g22390.1 (2006).
23. Evans, K. A. The redox budget of subduction zones. *Earth-Sci. Rev.* **113**, 11–32 (2012).
This paper quantifies a net flux of redox budget to the mantle at subduction zones capable of oxidizing the mantle wedge on Ma timescales but not yet the deep mantle on terrestrial timescales.
24. Carmichael, I. S. E. The redox states of basic and silicic magmas — a reflection of their source regions. *Contrib. Mineral. Petrol.* **106**, 129–141 (1991).
This paper suggests that the fO_2 recorded by volcanic rocks varies as a function of tectonic setting and reflects mantle fO_2.
25. Kelley, K. A. & Cottrell, E. Water and the oxidation state of subduction zone magmas. *Science* **325**, 605–607 (2009).
This paper showed that minimally degassed and primitive basalts erupted proximal to subduction zones record higher fO_2 than MORB and that this is true even when lithosphere and crust are thin or absent.
26. Wood, B. J., Bryndzia, L. T. & Johnson, K. E. Mantle oxidation-state and its relationship to tectonic environment and fluid speciation. *Science* **248**, 337–345 (1990).
This paper links the fO_2 recorded by peridotites to tectonic setting and plate tectonic processes, additionally inferring that, due to the relatively compressible nature of Fe^{3+}-bearing garnet, mantle in the garnet field would become progressively more reduced with depth.
27. Grocke, S. B., Cottrell, E., de Silva, S. & Kelley, K. A. The role of crustal and eruptive processes versus source variations in controlling the oxidation state of iron in central Andean magmas. *Earth Planet. Sci. Lett.* **440**, 92–104 (2016).
28. Crabtree, S. & Lange, R. An evaluation of the effect of degassing on the oxidation state of hydrous andesite and dacite magmas: a comparison of pre- and post-eruptive Fe^{2+} concentrations. *Contrib. Mineral. Petrol.* **2**, 209–224 (2012).
29. Tang, M., Erdman, M., Eldridge, G. & Lee, C. A. The redox 'filter' beneath magmatic orogens and the formation of continental crust. *Sci. Adv.* **4**, eaar4444 (2018).
30. Brounce, M., Kelley, K. A. & Cottrell, E. The $Fe^{3+}/\Sigma Fe$ variations in Mariana arc basalts and primary fO_2 of the mantle wedge. *J. Petrol.* **55**, 2513–2536 (2014).
31. Holycross, M. & Cottrell, E. Garnet crystallization does not drive oxidation at arcs. *Science* **380**, 506–509 (2023).
32. Brounce, M., Kelley, K. A., Cottrell, E. & Reagan, M. K. Temporal evolution of mantle wedge oxygen fugacity during subduction initiation. *Geology* **43**, 775–778 (2015).
This paper shows that the fO_2 recorded by mantle-derived melts increases by 1–2 orders of magnitude and reaches the fO_2 recorded by modern arc tholeiites within 1–2 million years of subduction initiation.
33. Brounce, M. et al. Covariation of slab tracers, volatiles, and oxidation during subduction initiation. *Geochem. Geophys. Geosyst.* https://doi.org/10.1029/2021gc009823 (2021).
34. Evans, K. A. & Tompkins, A. G. in *Magma Redox Geochemistry* (eds Neuville, D. R. & Moretti, R.) 63–92 (Wiley, 2021).
35. Li, Z. X. A. & Lee, C. T. A. The constancy of upper mantle fO_2 through time inferred from V/Sc ratios in basalts. *Earth Planet. Sci. Lett.* **228**, 483–493 (2004).
36. Delano, J. W. Redox history of the Earth's interior since ~3900 Ma: implications for prebiotic molecules. *Orig. Life Evol. Biosph.* **31**, 311–341 (2001).
37. Trail, D., Watson, E. B. & Tailby, N. D. The oxidation state of Hadean magmas and implications for early Earth's atmosphere. *Nature* **480**, 79–82 (2011).
38. Frost, D. J. et al. Experimental evidence for the existence of iron-rich metal in the Earth's lower mantle. *Nature* **428**, 409–412 (2004).
This paper experimentally demonstrates that disproportionation of FeO into core-forming iron metal alloy and Fe^{3+}-bearing perovskite could oxidize the Hadean mantle to modern fO_2 values as a natural consequence of core formation in a high-pressure silicate magma ocean.
39. Frost, D. J. & McCammon, C. A. The redox state of Earth's mantle. *Annu. Rev. Earth Planet. Sci.* **36**, 389–420 (2008).
This influential review of mantle oxygen fugacity through time and with depth in Earth's mantle includes a review of the sub-continental mantle and lower mantle.
40. Aulbach, S. & Stagno, V. Evidence for a reducing Archean ambient mantle and its effects on the carbon cycle. *Geology* **44**, 751–754 (2016).
41. Nicklas, R. W. et al. Secular mantle oxidation across the Archean-proterozoic boundary: evidence from V partitioning in komatiites and picrites. *Geochim. Cosmochim. Acta.* **250**, 49–75 (2019).
42. O'Neill, C. & Aulbach, S. Destabilization of deep oxidized mantle drove the great oxidation event. *Sci. Adv.* https://doi.org/10.1126/sciadv.abg1626 (2022).
43. Burnham, A. D., Miller, L. A. & Roskosz, M. A review of redox analytical methods in *Treatise on Geochemistry* 3rd edn (eds Anbar, A. & Weis, D.) 255–291 (Elsevier, 2025).
44. Herd, C. D. K. Basalts as probes of planetary interior redox state. *Rev. Mineral. Geochem.* **68**, 527–553 (2008).
45. Frost, B. R. in *Oxide Minerals: Petrologic and Magnetic Significance* (ed Lindsley, D. H.) 1–9 (BookCrafters Inc., 1991).
46. Zhang, H. L., Cottrell, E., Solheid, P. A., Kelley, K. A. & Hirschmann, M. M. Determination of $Fe^{3+}/\sum Fe$ of XANES basaltic glass standards by Mössbauer spectroscopy and its application to the oxidation state of iron in MORB. *Chem. Geol.* **479**, 166–175 (2018).
47. Cottrell, E. & Kelley, K. A. The oxidation state of Fe in MORB glasses and the oxygen fugacity of the upper mantle. *Earth Planet. Sci. Lett.* **305**, 270–282 (2011).
48. O'Neill, H. S. C., Berry, A. J. & Mallmann, G. The oxidation state of iron in mid-ocean ridge basaltic (MORB) glasses: implications for their petrogenesis and oxygen fugacities. *Earth Planet. Sci. Lett.* **504**, 152–162 (2018).
49. Berry, A. J., Stewart, G. A., O'Neill, H. S. C., Mallmann, G. & Mosselmans, J. F. W. A re-assessment of the oxidation state of iron in MORB glasses. *Earth Planet. Sci. Lett.* **483**, 114–123 (2018).
50. Bezos, A. & Humler, E. The $Fe^{3+}/\Sigma Fe$ ratios of MORB glasses and their implications for mantle melting. *Geochim. Cosmochim. Acta.* **69**, 711–725 (2005).
51. Kelemen, P. B., Shimizu, N. & Salters, V. J. M. Extraction of mid-ocean-ridge basalt from the upwelling mantle by focused flow of melt in dunite channels. *Nature* **375**, 747–753 (1995).
52. Davis, F. A. & Cottrell, E. Partitioning of Fe_2O_3 in peridotite partial melting experiments over a range of oxygen fugacities elucidates ferric iron systematics in mid-ocean ridge basalts and ferric iron content of the upper mantle. *Contrib. Mineral. Petrol.* https://doi.org/10.1007/s00410-021-01823-3 (2021).
53. Walter, M. & Cottrell, E. in *Treatise on Geochemistry* 3rd edn (eds Anbar, A. & Weis, D.) 231–273 (Elsevier, 2025).
54. Canil, D. et al. Ferric iron in peridotites and mantle oxidation-states. *Earth Planet. Sci. Lett.* **123**, 205–220 (1994).
This paper quantifies the distribution of Fe^{3+} in upper mantle minerals and shows that bulk rock Fe^{3+} does not correlate with fO_2 or extent of melting (F).
55. Gaetani, G. A. The behavior of $Fe^{3+}/\Sigma Fe$ during partial melting of spinel lherzolite. *Geochim. Cosmochim. Acta.* **185**, 64–77 (2016).
56. Bryndzia, L. T. & Wood, B. J. Oxygen thermobarometry of abyssal spinel peridotites — the redox state and C–O–H volatile composition of the Earth's sub-oceanic upper mantle. *Am. J. Sci.* **290**, 1093–1116 (1990).
57. Birner, S. K., Cottrell, E., Warren, J. M., Kelley, K. A. & Davis, F. A. Peridotites and basalts reveal broad congruence between two independent records of mantle fO_2 despite local redox heterogeneity. *Earth Planet. Sci. Lett.* **494**, 172–189 (2018).
58. Birner, S. K., Cottrell, E., Davis, F. A. & Warren, J. M. Deep, hot, ancient melting recorded by ultralow oxygen fugacity in peridotites. *Nature* **631**, 801–807 (2024).
59. Birner, S. K., Cottrell, E., Warren, J. M., Kelley, K. A. & Davis, F. A. Melt addition to mid-ocean ridge peridotites increases spinel Cr# with no significant effect on recorded oxygen fugacity. *Earth and Planet. Sci. Lett.* https://doi.org/10.1016/j.epsl.2021.116951 (2021).
60. Christie, D. M., Carmichael, I. S. E. & Langmuir, C. H. Oxidation-states of midocean ridge basalt glasses. *Earth Planet. Sci. Lett.* **79**, 397–411 (1986).
61. Woodland, A. B. & Koch, M. Variation in oxygen fugacity with depth in the upper mantle beneath the Kaapvaal craton, Southern Africa. *Earth Planet. Sci. Lett.* **214**, 295–310 (2003).
62. Ballhaus, C. & Frost, B. R. The generation of oxidized CO_2-bearing basaltic melts from reduced CH_4-bearing upper mantle sources. *Geochim. Cosmochim. Acta.* **58**, 4931–4940 (1994).
63. Moussallam, Y. et al. CO_2-undersaturated melt inclusions from the South West Indian ridge record surprisingly uniform redox conditions. *Geochem. Geophys. Geosyst.* https://doi.org/10.1029/2023gc011235 (2023).
64. Sorbadere, F. et al. The behaviour of ferric iron during partial melting of peridotite. *Geochim. Cosmochim. Acta* **239**, 235–254 (2018).
65. Davis, F. A. & Cottrell, E. Experimental investigation of basalt and peridotite oxybarometers: implications for spinel thermodynamic models and Fe^{3+} compatibility during generation of upper mantle melts. *Am. Mineral.* **103**, 1056–1067 (2018).
66. Dygert, N., Ustunisik, G. K. & Nielsen, R. L. Europium in plagioclase-hosted melt inclusions reveals mantle melting modulates oxygen fugacity. *Nat. Commun.* **15**, 3033 (2024).
67. Ghiorso, M. S. & Sack, R. O. Chemical mass-transfer in magmatic processes. 4. A revised and internally consistent thermodynamic model for the interpolation and extrapolation of liquid-solid equilibria in magmatic systems at elevated-temperatures and pressures. *Contrib. Mineral. Petrol.* **119**, 197–212 (1995).

68. Powell, R., Holland, T. & Worley, B. Calculating phase diagrams involving solid solutions via non-linear equations, with examples using THERMOCALC. *J. Metamorph. Geol.* **16**, 577–588 (1998).
69. Stolper, E. M., Shorttle, O., Antoshechkina, P. M. & Asimow, P. D. The effects of solid-solid phase equilibria on the oxygen fugacity of the upper mantle. *Am. Mineral.* **105**, 1445–1471 (2020).
70. Tomlinson, E. L. & Holland, T. J. B. A thermodynamic model for the subsolidus evolution and melting of peridotite. *J. Petrol.* https://doi.org/10.1093/petrology/egab012 (2021).
71. Zhang, F. et al. The constant oxidation state of Earth's mantle since the Hadean. *Nat. Commun.* **15**, 6521 (2024).
72. Cottrell, E. et al. in *Magma Redox Geochemistry, Geophysical Monograph 266* (eds Neuville, D. R. & Moretti, R.) 33–61 (Wiley, 2021).
73. Lee, C.-T., Leeman, W. P., Canil, D. & Li, Z.-X. A. Similar V/Sc systematics in MORB and arc basalts: implications for the oxygen fugacities of their mantle source regions. *J. Petrol.* **46**, 2313–2336 (2005).
Based on V/Sc, this paper suggests that mantle fO_2 beneath ridges and arcs is indistinguishable and that arc magmas become oxidized in the crust, prompting renewed interest in mantle fO_2.
74. Ague, J. J. & Brimhall, G. H. Granites of the batholiths of California: products of local assimilation and regional-scale crustal contamination. *Geology* **15**, 63–66 (1987).
75. Farner, M. J. & Lee, C.-T. A. Effects of crustal thickness on magmatic differentiation in subduction zone volcanism: a global study. *Earth Planet. Sci. Lett.* **470**, 96–107 (2017).
76. Kelley, K. A. & Cottrell, E. The influence of magmatic differentiation on the oxidation state of Fe in a basaltic arc magma. *Earth Planet. Sci. Lett.* **329**, 109–121 (2012).
77. Moussallam, Y. et al. Tracking the changing oxidation state of Erebus magmas, from mantle to surface, driven by magma ascent and degassing. *Earth Planet. Sci. Lett.* **393**, 200–209 (2014).
78. Métrich, N. Redox state of volatiles and their relationships with iron in silicate melts: implications for magma degassing. *Magma Redox Geochemistry* **266**, 215–232 (2021).
79. Brounce, M., Stolper, E. & Eiler, J. Redox variations in Mauna Kea lavas, the oxygen fugacity of the Hawaiian plume, and the role of volcanic gases in Earth's oxygenation. *Proc. Natl Acad. Sci. USA* **114**, 8997–9002 (2017).
80. Muth, M. J. & Wallace, P. J. Slab-derived sulfate generates oxidized basaltic magmas in the southern cascade arc (California, USA). *Geology* https://doi.org/10.1130/g48759.1 (2021).
81. Bucholz, C. E. & Kelemen, P. B. Oxygen fugacity at the base of the Talkeetna arc, Alaska. *Contrib. Mineral. Petrol.* https://doi.org/10.1007/s00410-019-1609-z (2019).
82. Sosa, E. S. et al. Petrology and geochemistry of Adak Island plutonic xenoliths: implications for primitive magma generation and crustal differentiation in the Aleutian Island arc. *J. Petrol.* https://doi.org/10.1093/petrology/egad073 (2023).
83. Parkinson, I. J. & Pearce, J. A. Peridotites from the Izu–Bonin–Mariana forearc (ODP Leg 125): evidence for mantle melting and melt–mantle interaction in a supra-subduction zone setting. *J. Petrol.* **39**, 1577–1618 (1998).
84. Pearce, J. A., Barker, P. F., Edwards, S. J., Parkinson, I. J. & Leat, P. T. Geochemistry and tectonic significance of peridotites from the south sandwich arc±basin system, South Atlantic. *Contrib. Mineral. Petrol.* **139**, 36–53 (2000).
85. Birner, S. K. et al. Forearc peridotites from Tonga record heterogeneous oxidation of the mantle following subduction initiation. *J. Petrol.* **58**, 1755–1780 (2017).
86. Benard, A. et al. Oxidising agents in sub-arc mantle melts link slab devolatilisation and arc magmas. *Nat. Commun.* https://doi.org/10.1038/s41467-018-05804-2 (2018).
87. Brounce, M., Stolper, E. & Eiler, J. The mantle source of basalts from Reunion Island is not more oxidized than the MORB source mantle. *Contrib. Mineral. Petrol.* **177**, 1–18 (2022).
88. Davis, F. A., Cottrell, E., Birner, S. K., Warren, J. M. & Lopez, O. G. Revisiting the electron microprobe method of spinel-olivine-orthopyroxene oxybarometry applied to spinel peridotitesk. *Am. Mineral.* **102**, 421–435 (2017).
89. Mallmann, G., Burnham, A. & Fonseca, R. O. in *Magma Redox Geochemistry, Geophysical Monograph 266* (eds Neuville, D. R. & Moretti, R.) 345–367 (Wiley, 2021).
90. Sutton, S. R. et al. Vanadium K edge XANES of synthetic and natural basaltic glasses and application to microscale oxygen barometry. *Geochim. Cosmochim. Acta* **69**, 2333–2348 (2005).
91. Shervais, J. W. Ti–V plots and the petrogenesis of modern and ophiolitic lavas. *Earth Planet. Sci. Lett.* **59**, 101–118 (1982).
92. Wang, J. et al. Oxidation state of arc mantle revealed by partitioning of V, Sc, and Ti between mantle minerals and basaltic melts. *J. Geophys. Res. Solid Earth* **124**, 4617–4638 (2019).
93. Laubier, M., Grove, T. L. & Langmuir, C. H. Trace element mineral/melt partitioning for basaltic and basaltic andesitic melts: an experimental and laser ICP-MS study with application to the oxidation state of mantle source regions. *Earth Planet. Sci. Lett.* **392**, 265–278 (2014).
94. Mallmann, G. & O'Neill, H. S. C. The crystal/melt partitioning of V during mantle melting as a function of oxygen fugacity compared with some other elements (Al, P, Ca, Sc, Ti, Cr, Fe, Ga, Y, Zr and Nb). *J. Petrol.* **50**, 1765–1794 (2009).
95. Leuthold, J., Blundy, J. & Ulmer, P. Trace element partitioning in basaltic systems as a function of oxygen fugacity. *Contrib. Mineral. Petrol.* **178**, 95 (2023).
96. Canil, D. & Fedortchouk, Y. Olivine–liquid partitioning of vanadium and other trace elements, with applications to modern and ancient picrites. *Can. Mineral.* **39**, 319–330 (2001).
97. Shervais, J. W. The petrogenesis of modern and ophiolitic lavas reconsidered: Ti–V and Nb–Th. *Geosci. Front.* **13**, 101319 (2022).
98. Liu, C.-T., Ye, C.-Y. & ZhangZhou, J. Modelling redox state via V-Sc-Ti-Yb partitioning in mantle derived melts. *Geochem. Perspect. Lett.* **33**, 56–62 (2025).
99. Yang, A. Y. et al. A subduction influence on ocean ridge basalts outside the Pacific subduction shield. *Nat. Commun.* **12**, 4757 (2021).
100. Turner, S. J. & Langmuir, C. H. A quantitative framework for global variations in arc geochemistry. *Earth Planet. Sci. Lett.* https://doi.org/10.1016/j.epsl.2022.117411 (2022).
101. Kelley, K. A. et al. Mantle melting as a function of water content beneath the Mariana arc. *J. Petrol.* **51**, 1711–1738 (2010).
102. Pertermann, M., Hirschmann, M. M., Hametner, K., Günther, D. & Schmidt, M. W. Experimental determination of trace element partitioning between garnet and silica-rich liquid during anhydrous partial melting of MORB-like eclogite. *Geochem. Geophys. Geosyst.* https://doi.org/10.1029/2003gc000638 (2004).
103. Yogodzinski, G. M. et al. The role of subducted basalt in the source of island arc magmas: evidence from seafloor lavas of the Western Aleutians. *J. Petrol.* **56**, 441–492 (2015).
104. Hofmann, A. W. & White, W. M. Mantle plumes from ancient oceanic crust. *Earth Planet. Sci. Lett.* **57**, 421–436 (1982).
105. Hauri, E. et al. in *Earth's Deep Carbon: Past to Present* (eds Orcutt, B., Daniel, I. & Dasgupta, R.) 237–275 (Cambridge Univ. Press, 2019).
106. Wallace, P. J. Volatiles in subduction zone magmas: concentrations and fluxes based on melt inclusion and volcanic gas data. *J. Volcanol. Geotherm. Res.* **140**, 217–240 (2005).
107. Canil, D. & Fellows, S. A. Sulphide–sulphate stability and melting in subducted sediment and its role in arc mantle redox and chalcophile cycling in space and time. *Earth Planet. Sci. Lett.* **470**, 73–86 (2017).
108. Muth, M. & Wallace, P. Sulfur recycling in subduction zones and the oxygen fugacity of mafic arc magmas. *Earth Planet. Sci. Lett.* **599**, 117836 (2022).
109. Jenner, F. E., O'Neill, H. S. C., Arculus, R. J. & Mavrogenes, J. A. The magnetite crisis in the evolution of arc-related magmas and the initial concentration of Au, Ag and Cu. *J. Petrol.* **51**, 2443–2464 (2010).
110. Zhao, Y., Yang, A. Y., Langmuir, C. & Zhao, T.-P. Oxidized primary arc magmas: constraints from Cu/Zr systematics in global arc volcanics. *Sci. Adv.* **8**, 9 (2022).
111. Elliott, T., Plank, T., Zindler, A., White, W. & Bourdon, B. Element transport from slab to volcanic front at the Mariana arc. *J. Geophys. Res. Solid Earth* **102**, 14991–15019 (1997).
112. Pearce, J. A. in *Continental basalts and mantle xenoliths* (eds Hawkesworth, C. J. & Norry, M. J.) 230–249 (1983).
113. Evans, K., Elburg, M. & Kamenetsky, V. Oxidation state of subarc mantle. *Geology* **40**, 783–786 (2012).
114. Brounce, M., Cottrell, E. & Kelley, K. A. The redox budget of the Mariana subduction zone. *Earth Planet. Sci. Lett.* **528**, 115859 (2019).
115. Blatter, D. L., Sisson, T. W. & Hankins, W. B. Garnet stability in arc basalt, andesite, and dacite — an experimental study. *Contrib. Mineral. Petrol.* https://doi.org/10.1007/s00410-023-02008-w (2023).
116. Pons, M. L., Debret, B., Bouilhol, P., Delacour, A. & Williams, H. Zinc isotope evidence for sulfate-rich fluid transfer across subduction zones. *Nat. Commun.* **7**, 13794 (2016).
117. Lecuyer, C. & Ricard, Y. Long-term fluxes and budget of ferric iron: implication for the redox states of the Earth's mantle and atmosphere. *Earth Planet. Sci. Lett.* **165**, 197–211 (1999).
118. Tollan, P. & Hermann, J. Arc magmas oxidised by water dissociation and hydrogen incorporation in orthopyroxene. *Nat. Geosci.* **12**, 667–671 (2019).
119. Brandon, A. D. & Draper, D. S. Constraints on the origin of the oxidation state of mantle overlying subduction zones: an example from Simcoe, Washington, USA. *Geochim. Cosmochim. Acta* **60**, 1739–1749 (1996).
120. Botcharnikov, R. E., Koepke, J., Holtz, F., McCammon, C. & Wilke, M. The effect of water activity on the oxidation and structural state of Fe in a ferro-basaltic melt. *Geochim. Cosmochim. Acta* **69**, 5071–5085 (2005).
121. Peslier, A. H., Luhr, J. F. & Post, J. Low water contents in pyroxenes from spinel-peridotites of the oxidized, sub-arc mantle wedge. *Earth Planet. Sci. Lett.* **201**, 69–86 (2002).
122. Frost, B. R. & Ballhaus, C. Comment on 'Constraints on the origin of the oxidation state of mantle overlying subduction zones: an example from Simcoe, Washington, USA'. *Geochim. Cosmochim. Acta* **62**, 329–331 (1998).
123. Tumiati, S., Godard, G., Martin, S., Malaspina, N. & Poli, S. Ultra-oxidized rocks in subduction mélanges? Decoupling between oxygen fugacity and oxygen availability in a Mn-rich metasomatic environment. *Lithos* **226**, 116–130 (2015).
124. Pokrovski, G. S. & Dubrovinsky, L. S. The S_3^- ion is stable in geological fluids at elevated temperatures and pressures. *Science* **331**, 1052–1054 (2011).
125. Evans, K. A. & Frost, B. R. Deserpentinization in subduction zones as a source of oxidation in arcs: a reality check. *J. Petrol.* https://doi.org/10.1093/petrology/egab016 (2021).
126. Kelemen, P. B. & Manning, C. E. Reevaluating carbon fluxes in subduction zones, what goes down, mostly comes up. *Proc. Natl Acad. Sci. USA* **112**, E3997–E4006 (2015).
127. Ague, J. J. et al. Slab-derived devolatilization fluids oxidized by subducted metasedimentary rocks. *Nat. Geosci.* https://doi.org/10.1038/s41561-022-00904-7 (2022).
128. Evans, K. A. & Tomkins, A. G. The relationship between subduction zone redox budget and arc magma fertility. *Earth Planet. Sci. Lett.* https://doi.org/10.1016/j.epsl.2011.06.009 (2011).
129. Jégo, S. & Dasgupta, R. The fate of sulfur during fluid-present melting of subducting basaltic crust at variable oxygen fugacity. *J. Petrol.* **55**, 1019–1050 (2014).
130. Gaillard, F., Scaillet, B., Pichavant, M. & Iacono-Marziano, G. The redox geodynamics linking basalts and their mantle sources through space and time. *Chem. Geol.* **418**, 217–233 (2015).
131. Wykes, J. L., Newton, R. C. & Manning, C. E. Solubility of andradite, $Ca_3Fe_2Si_3O_{12}$, in a 10 mol% NaCl solution at 800 °C and 10 kbar: implications for the metasomatic origin of grandite garnet in calc-silicate granulites. *Am. Mineral.* **93**, 886–892 (2008).
132. Gammons, C. & Seward, T. Stability of manganese (II) chloride complexes from 25 to 300 °C. *Geochim. Cosmochim. Acta* **60**, 4295–4311 (1996).

133. Tiraboschi, C. et al. Preferential mobilisation of oxidised iron by slab-derived hydrous silicate melts. *Geochemical Perspect. Lett.* **24**, 43–47 (2023).
134. Schettino, E. & Poli, S. in *Carbon in Earth's Interior.* (eds Manning, C. E., Lin, J.-F. & Mao, W. L.) 209–221 (Geophysical Monograph Series, 2020).
135. Poli, S., Franzolin, E., Fumagalli, P. & Crottini, A. The transport of carbon and hydrogen in subducted oceanic crust: an experimental study to 5 GPa. *Earth Planet. Sci. Lett.* **278**, 350–360 (2009).
136. Facq, S., Daniel, I., Montagnac, G., Cardon, H. & Sverjensky, D. A. In situ Raman study and thermodynamic model of aqueous carbonate speciation in equilibrium with aragonite under subduction zone conditions. *Geochim. Cosmochim. Acta* **132**, 375–390 (2014).
137. Tumiati, S. et al. Silicate dissolution boosts the CO_2 concentrations in subduction fluids. *Nat. Commun.* **8**, 616 (2017).
138. Sverjensky, D. A., Stagno, V. & Huang, F. Important role for organic carbon in subduction-zone fluids in the deep carbon cycle. *Nat. Geosci.* **7**, 909–913 (2014).
139. Debret, B. & Sverjensky, D. A. Highly oxidising fluids generated during serpentinite breakdown in subduction zones. *Sci. Rep.* **7**, 10351 (2017).
140. Debret, B. et al. Evolution of Fe redox state in serpentine during subduction. *Earth Planet. Sci. Lett.* **400**, 206–218 (2014).
141. Evans, K. A., Reddy, S. M., Tomkins, A. G., Crossley, R. J. & Frost, B. R. Effects of geodynamic setting on the redox state of fluids released by subducted mantle lithosphere. *Lithos* **278–281**, 26–42 (2017).
142. Piccoli, F. et al. Subducting serpentinites release reduced, not oxidized, aqueous fluids. *Sci. Rep.* **9**, 19573 (2019).
143. Stamper, C. et al. Oxidised phase relations of a primitive basalt from Grenada, Lesser Antilles. *Contrib. Mineral. Petrol.* **167**, 954 (2014).
144. Behn, M. D., Kelemen, P. B., Hirth, G., Hacker, B. R. & Massonne, H.-J. Diapirs as the source of the sediment signature in arc lavas. *Nat. Geosci.* **4**, 641–646 (2011).
145. Song, S. et al. Oxidation of arcs and mantle wedges by reduction of manganese in pelagic sediments during seafloor subduction. *Am. Mineral.* **107**, 1850–1857 (2022).
146. Cannaò, E. & Malaspina, N. From oceanic to continental subduction: implications for the geochemical and redox evolution of the supra-subduction mantle. *Geosphere* **14**, 2311–2336 (2018).
147. Consuma, G. et al. Multi-stage sulfur and carbon mobility in fossil continental subduction zones: new insights from carbonate-bearing orogenic peridotites. *Geochim. Cosmochim. Acta* **306**, 143–170 (2021).
148. Laborda-López, C. et al. Geochemical evolution of rodingites during subduction: insights from Cerro del Almirez (southern Spain). *Lithos* https://doi.org/10.1016/j.lithos.2020.105639 (2020).
149. Schwarzenbach, E. M. et al. Sulphur and carbon cycling in the subduction zone melange. *Sci. Rep.* **8**, 15517 (2018).
150. Menzel, M. D., Garrido, C. J. & López Sánchez-Vizcaíno, V. Fluid-mediated carbon release from serpentinite-hosted carbonates during dehydration of antigorite-serpentinite in subduction zones. *Earth Planet. Sci. Lett.* https://doi.org/10.1016/j.epsl.2019.115964 (2020).
151. Padrón-Navarta, J. A., López Sánchez-Vizcaíno, V., Menzel, M. D., Gómez-Pugnaire, M. T. & Garrido, C. J. Mantle wedge oxidation from deserpentinization modulated by sediment-derived fluids. *Nat. Geosci.* **16**, 268–275 (2023).
152. D'Souza, R. J. & Canil, D. The partitioning of chalcophile elements between sediment melts and fluids at 3 GPa, 950–1050 °C with implications for slab fluids in subduction zones. *Earth Planet. Sci. Lett.* **498**, 215–225 (2018).
153. Xu, Z. & Li, Y. The sulfur concentration at anhydrite saturation in silicate melts: implications for sulfur cycle and oxidation state in subduction zones. *Geochim. Cosmochim. Acta* **306**, 98–123 (2021).
154. Gerrits, A. R. et al. Release of oxidizing fluids in subduction zones recorded by iron isotope zonation in garnet. *Nat. Geosci.* **12**, 1029–1033 (2019).
155. Walters, J. B., Cruz-Uribe, A. M. & Marschall, H. R. Sulfur loss from subducted altered oceanic crust and implications for mantle oxidation. *Geochem. Perspect. Lett.* **13**, 36–41 (2020).
156. Hall, P. S. & Kincaid, C. Diapiric flow at subduction zones: a recipe for rapid transport. *Science* **292**, 2472–2475 (2001).
157. Marschall, H. R. & Schumacher, J. C. Arc magmas sourced from mélange diapirs in subduction zones. *Nat. Geosci.* **5**, 862–867 (2012).
158. Maunder, B., van Hunen, J., Magni, V. & Bouilhol, P. Relamination of mafic subducting crust throughout Earth's history. *Earth Planet. Sci. Lett.* **449**, 206–216 (2016).
159. Maierová, P., Schulmann, K. & Gerya, T. Relamination styles in collisional orogens. *Tectonics* **37**, 224–250 (2018).
160. Shirey, S. B., Wagner, L. S., Walter, M. J., Pearson, D. G. & van Keken, P. E. Slab transport of fluids to deep focus earthquake depths—thermal modeling constraints and evidence from diamonds. *AGU Adv.* **2**, e2020AV000304 (2021).
161. Halpaap, F. et al. Earthquakes track subduction fluids from slab sourceto mantle wedge sink. *Sci. Adv.* **5**, eaav7369 (2019).
162. Lyons, T. W., Reinhard, C. T. & Planavsky, N. J. The rise of oxygen in Earth's early ocean and atmosphere. *Nature* **506**, 307–315 (2014).
163. Holland, H. D. Volcanic gases, black smokers, and the great oxidation event. *Geochim. Cosmochim. Acta* **66**, 3811–3826 (2002).
164. Holland, H. D. *The Chemistry of the Atmosphere and Oceans* (Wiley Interscience, 1978).
165. Kasting, J. F., Eggler, D. H. & Raeburn, S. P. Mantle redox evolution and the oxidation-state of the Archean atmosphere. *J. Geol.* **101**, 245–257 (1993).
166. Moussallam, Y., Oppenheimer, C. & Scaillet, B. On the relationship between oxidation state and temperature of volcanic gas emissions. *Earth Planet. Sci. Lett.* **520**, 260–267 (2019).
167. Kadoya, S., Catling, D. C., Nicklas, R. W., Puchtel, I. S. & Anbar, A. D. Mantle cooling causes more reducing volcanic gases and gradual reduction of the atmosphere. *Geochem. Perspect. Lett.* **13**, 25–29 (2020).
168. Gaillard, F., Scaillet, B. & Arndt, N. T. Atmospheric oxygenation caused by a change in volcanic degassing pressure. *Nature* **478**, 229–232 (2011).
169. Kump, L. R. & Barley, M. E. Increased subaerial volcanism and the rise of atmospheric oxygen 2.5 billion years ago. *Nature* **448**, 1033–1036 (2007).
170. Hill, R. & Roeder, P. The crystallization of spinel from basaltic liquid as a function of oxygen fugacity. *J. Geol.* **82**, 709–729 (1974).
171. Rollinson, H., Adetunji, J., Lenaz, D. & Szilas, K. Archaean chromitites show constant $Fe^{3+}/\Sigma Fe$ in Earth's asthenospheric mantle since 3.8 Ga. *Lithos* **282–283**, 316–325 (2017).
172. Nicklas, R. W., Puchtel, I. S. & Ash, R. D. High-precision determination of the oxidation state of komatiite lavas using vanadium liquid-mineral partitioning. *Chem. Geol.* **433**, 36–45 (2016).
173. Nicklas, R. W., Puchtel, I. S. & Baxter, E. F. Concordance of V-in-olivine and Fe-XANES oxybarometry methods in mid-ocean ridge basalts. *Earth Planet. Sci. Lett.* https://doi.org/10.1016/j.epsl.2023.118492 (2024).
174. Nicklas, R. W. et al. Oxidized mantle sources of HIMU- and EM-type Ocean Island basalts. *Chem. Geol.* https://doi.org/10.1016/j.chemgeo.2022.120901 (2022).
175. McDonough, W. F. & Ireland, T. R. Intraplate origin of komatiites inferred from trace elements in glass inclusions. *Nature* **365**, 432–434 (1993).
176. Sobolev, A. V. et al. Komatiites reveal a hydrous Archaean deep-mantle reservoir. *Nature* **531**, 628–632 (2016).
177. Asafov, E. et al. Belingwe komatiites (2.7 Ga) originate from a plume with moderate water content, as inferred from inclusions in olivine. *Chem. Geol.* **478**, 39–59 (2018).
178. Sobolev, A. V. et al. Deep hydrous mantle reservoir provides evidence for crustal recycling before 3.3 billion years ago. *Nature* **571**, 555–559 (2019).
179. Berry, A. J. et al. Oxidation state of iron in komatiitic melt inclusions indicates hot Archaean mantle. *Nature* **455**, 960–963 (2008).
180. Bucholz, C. E., Gaetani, G. A., Behn, M. D. & Shimizu, N. Post-entrapment modification of volatiles and oxygen fugacity in olivine-hosted melt inclusions. *Earth Planet. Sci. Lett.* **374**, 145–155 (2013).
181. Humphreys, J., Brounce, M. & Walowski, K. Diffusive equilibration of H_2O and oxygen fugacity in natural olivine-hosted melt inclusions. *Earth Planet. Sci. Lett.* https://doi.org/10.1016/j.epsl.2022.117409 (2022).
182. Canil, D. Vanadium in peridotites, mantle redox and tectonic environments: Archean to present. *Earth Planet. Sci. Lett.* **195**, 75–90 (2002).
183. Arndt, N., Lesher, M. C. & Barnes, S. J. *Komatiite* (Cambridge Univ. Press, 2008).
184. Herzberg, C., Condie, K. & Korenaga, J. Thermal history of the Earth and its petrological expression. *Earth Planet. Sci. Lett.* **292**, 79–88 (2010).
185. Aulbach, S. & Viljoen, K. S. Eclogite xenoliths from the Lace kimberlite, Kaapvaal craton: from convecting mantle source to palaeo-ocean floor and back. *Earth Planet. Sci. Lett.* **431**, 274–286 (2015).
186. Jacob, D. Nature and origin of eclogite xenoliths from kimberlites. *Lithos* **77**, 295–316 (2004).
187. Smart, K. A. et al. Tectonic significance and redox state of paleoproterozoic eclogite and pyroxenite components in the slave cratonic mantle lithosphere, Voyageur kimberlite, Arctic Canada. *Chem. Geol.* **455**, 98–119 (2017).
188. Barth, M. G. et al. Geochemistry of xenolithic eclogites from West Africa, Part I: a link between low MgO eclogites and Archean crust formation. *Geochim. Cosmochim. Acta* **65**, 1499–1527 (2001).
189. Aulbach, S., Woodland, A. B., Vasilyev, P., Galvez, M. E. & Viljoen, K. S. Effects of low-pressure igneous processes and subduction on Fe3+/ΣFe and redox state of mantle eclogites from Lace (Kaapvaal craton). *Earth Planet. Sci. Lett.* **474**, 283–295 (2017).
190. Marras, G., Mikhailenko, D., McCammon, C. A., Agasheva, E. & Stagno, V. Ferric iron in eclogitic garnet and clinopyroxene from the V. Grib kimberlite pipe (NW Russia): evidence of a highly oxidized subducted slab. *J. Petrol.* https://doi.org/10.1093/petrology/egae054 (2024).
191. Aulbach, S. & Smart, K. A. Petrogenesis and geodynamic significance of xenolithic eclogites. *Annu. Rev. Earth Planet. Sci.* **51**, 521–549 (2023).
192. Herzberg, C. Origin of high-Mg bimineralic eclogite xenoliths in kimberlite: a comment on a paper by Aulbach and Arndt (2019). *Earth Planet. Sci. Lett.* **510**, 231–233 (2019).
193. Aulbach, S. & Arndt, N. T. Eclogites as palaeodynamic archives: evidence for warm (not hot) and depleted (but heterogeneous) Archaean ambient mantle. *Earth Planet. Sci. Lett.* **505**, 162–172 (2019).
194. Stagno, V. & Aulbach, S. in *Magma Redox Geochemistry* (eds Neuville, D. R. & Moretti, R.) 19–32 (Wiley, 2021).
195. Condie, K. Changing tectonic settings through time: indiscriminate use of geochemical discriminant diagrams. *Precambrian Res.* **266**, 587–591 (2015).
196. Condie, K. C. & Shearer, C. K. Tracking the evolution of mantle sources with incompatible element ratios in stagnant-lid and plate-tectonic planets. *Geochim. Cosmochim. Acta* **213**, 47–62 (2017).
197. Gao, L. et al. Oxidation of Archean upper mantle caused by crustal recycling. *Nat. Commun.* **13**, 3283 (2022).
198. Herzberg, C. & Asimow, P. D. Petrology of some oceanic island basalts: PRIMELT2.XLS software for primary magma calculation. *Geochem. Geophys. Geosyst.* https://doi.org/10.1029/2008gc002057 (2008).
199. Barnes, S. J., Williams, M., Smithies, R. H., Hanski, E. & Lowrey, J. R. Trace element contents of mantle-derived magmas through time. *J. Petrol.* https://doi.org/10.1093/petrology/egab024 (2021).

200. Nimmo, F. & Kleine, T. in *The Early Earth: Accretion and Differentiation* (eds Badro, J. & Walter, M. J.) 83–102 (AGU, 2015).
201. Elkins-Tanton, L. T. Magma oceans in the inner solar system. *Annu. Rev. Earth Planet. Sci.* **40**, 113–139 (2012).
202. Rubie, D. C. et al. Heterogeneous accretion, composition and core–mantle differentiation of the Earth. *Earth Planet. Sci. Lett.* **301**, 31–42 (2011).
203. Siebert, J., Badro, J., Antonangeli, D. & Ryerson, F. J. Terrestrial accretion under oxidizing conditions. *Science* **339**, 1194–1197 (2013).
204. Elkins-Tanton, L. T. Linked magma ocean solidification and atmospheric growth for Earth and Mars. *Earth Planet. Sci. Lett.* **271**, 181–191 (2008).
205. Pahlevan, K., Schaefer, L. & Hirschmann, M. M. Hydrogen isotopic evidence for early oxidation of silicate Earth. *Earth Planet Sci Lett* https://doi.org/10.1016/j.epsl.2019.115770 (2019).
206. Smythe, D. J. & Brenan, J. M. Magmatic oxygen fugacity estimated using zircon-melt partitioning of cerium. *Earth Planet. Sci. Lett.* **453**, 260–266 (2016).
207. O'Neill, H. S. The origin of the moon and the early history of the earth — a chemical model. Part 2: the Earth. *Geochim. Cosmochim. Acta* **55**, 1159–1172 (1991).
208. Wanke, H. Constitution of terrestrial planets. *Philos. Trans. R. Soc. Lond. Ser. A* **303**, 287–302 (1981).
209. Chambers, J. E. Planetary accretion in the inner solar system. *Earth Planet. Sci. Lett.* **223**, 241–252 (2004).
210. Hunten, D. M. Escape of light gases from planetary atmospheres. *J. Atmos. Sci.* **30**, 1481–1494 (1973).
211. Sharp, Z. D., McCubbin, F. M. & Shearer, C. K. A hydrogen-based oxidation mechanism relevant to planetary formation. *Earth Planet. Sci. Lett.* **380**, 88–97 (2013).
212. Catling, D. C., Zahnle, K. J. & McKay, C. P. Biogenic methane, hydrogen escape, and the irreversible oxidation of early Earth. *Science* **293**, 839–843 (2001).
213. Young, E. D., Shahar, A. & Schlichting, H. E. Earth shaped by primordial H_2 atmospheres. *Nature* **616**, 306–311 (2023).
214. Javoy, M. The integral enstatite chondrite model of the Earth. *Geophys. Res. Lett.* **22**, 2219–2222 (1995).
215. Badro, J., Brodholt, J. P., Piet, H., Siebert, J. & Ryerson, F. J. Core formation and core composition from coupled geochemical and geophysical constraints. *Proc. Natl Acad. Sci. USA* **112**, 12310–12314 (2015).
216. Frost, D. J., Mann, U., Asahara, Y. & Rubie, D. C. The redox state of the mantle during and just after core formation. *Philos. Trans. A Math. Phys. Eng. Sci.* **366**, 4315–4337 (2008).
217. O'Neill, H. S. C. et al. An experimental determination of the effect of pressure on the $Fe^{3+}/\Sigma Fe$ ratio of an anhydrous silicate melt to 3.0 GPa. *Am. Mineral.* **91**, 404–412 (2006).
218. Zhang, H., Hirschmann, M., Cottrell, E. & Withers, A. Effect of pressure on $Fe^{3+}/\Sigma Fe$ ratio in a mafic magma and consequences for magma ocean redox gradients. *Geochim. Cosmochim. Acta* **204**, 83–103 (2017).
219. Armstrong, K., Frost, D. J., McCammon, C., Rubie, D. C. & Ballaran, T. B. Deep magma ocean formation set the oxidation state of Earth's mantle. *Science* **365**, 903–906 (2019).
220. Zhang, H. L. et al. Ferric iron stabilization at deep magma ocean conditions. *Sci. Adv.* **10**, eadp1752 (2024).
221. Kuwahara, H., Nakada, R., Kadoya, S., Yoshino, T. & Irifune, T. Hadean mantle oxidation inferred from melting of peridotite under lower-mantle conditions. *Nat. Geosci.* **16**, 461–465 (2023).
222. Deng, J., Du, Z., Karki, B. B., Ghosh, D. B. & Lee, K. K. A magma ocean origin to divergent redox evolutions of rocky planetary bodies and early atmospheres. *Nat. Commun.* **11**, 2007 (2020).
223. Hirschmann, M. Magma oceans, iron and chromium redox, and the origin of comparatively oxidized planetary mantles. *Geochim. Cosmochim. Acta* **328**, 221–241 (2022).
224. Sossi, P. A. et al. Redox state of Earth's magma ocean and its Venus-like early atmosphere. *Sci. Adv.* **6**, eabd1387 (2020).
225. Hirschmann, M. M. The deep Earth oxygen cycle: mass balance considerations on the origin and evolution of mantle and surface oxidative reservoirs. *Earth Planet. Sci. Lett.* https://doi.org/10.1016/j.epsl.2023.118311 (2023).
226. Lichtenberg, T. et al. Vertically resolved magma ocean–protoatmosphere evolution: H_2, H_2O, CO_2, CH_4, CO, O_2, and N_2 as primary absorbers. *J. Geophys. Res. Planet.* **126**, e2020JE006711 (2021).
227. Bower, D. J., Hakim, K., Sossi, P. A. & Sanan, P. Retention of water in terrestrial magma oceans and carbon-rich early atmospheres. *Planet. Sci. J.* **3**, 93 (2022).
228. Cottrell, E. et al. *Oxygen Fugacity Across Tectonic Settings v.2, Version 1.0* (Interdisciplinary Earth Data Alliance, accessed 9 October 2025); https://doi.org/10.60520/IEDA/113694.
229. Cottrell, E. *Vanadium Redox Proxy Applied to Modern Mantle-Derived Magmas, Version 1.0* (Interdisciplinary Earth Data Alliance, accessed 9 October 2025); https://doi.org/10.60520/IEDA/113251.
230. Canil, D. *Vanadium Redox Proxies Applied to Mantle-derived magmas over time. Version. 1.0* https://doi.org/10.26022/IEDA/112512 (2023).
231. Cottrell, E. et al. Oxygen fugacity across tectonic settings, version 1.0. https://doi.org/10.26022/IEDA/111899 (IEDA, 2021).
232. Andrys, J. L., Cottrell, E., Kelley, K. A., Waters, L. E. & Coombs, M. L. Insights on arc magmatic systems drawn from natural melt inclusions and crystallization experiments at P_{H_2O} = 800 MPa under oxidizing conditions. *J. Petrol.* **65**, egae117 (2024).
233. O'Neill, H. S. C. et al. The relationship between iron redox states and H2O contents in back-arc basin basaltic glasses from the North Fiji Basin. *Chem. Geol.* **655**, 122062 (2024).
234. Moussallam, Y. et al. CO2-undersaturated melt inclusions from the south west Indian ridge record surprisingly uniform redox conditions. *Geochem. Geophys. Geosyst.* **24**, e2023GC011235 (2023).
235. Brounce, M., Scoggins, S., Fischer, T. P., Ford, H. & Byrnes, J. Volatiles and redox along the East African Rift. *Geochem. Geophys. Geosyst.* **25**, e2024GC011657 (2024).
236. Moussallam, Y. et al. Mantle plumes are oxidised. *Earth Planet. Sci. Lett.* https://doi.org/10.1016/j.epsl.2019.115798 (2019).
237. Hartley, M. E., Shorttle, O., Maclennan, J., Moussallam, Y. & Edmonds, M. Olivine-hosted melt inclusions as an archive of redox heterogeneity in magmatic systems. *Earth Planet. Sci. Lett.* **479**, 192–205 (2017).
238. Moussallam, Y. et al. The impact of degassing on the oxidation state of basaltic magmas: a case study of Kilauea volcano. *Earth Planet. Sci. Lett.* **450**, 317–325 (2016).
239. Shorttle, O. et al. Fe-XANES analyses of Reykjanes Ridge basalts: implications for oceanic crust's role in the solid Earth oxygen cycle. *Earth Planet. Sci. Lett.* **427**, 272–285 (2015).
240. Gale, A., Laubier, M., Escrig, S. & Langmuir, C. H. Constraints on melting processes and plume-ridge interaction from comprehensive study of the FAMOUS and north famous segments, Mid-Atlantic ridge. *Earth Planet. Sci. Lett.* **365**, 209–220 (2013).
241. Turner, S. J. & Langmuir, C. H. The global chemical systematics of arc front stratovolcanoes: evaluating the role of crustal processes. *Earth Planet. Sci. Lett.* **422**, 182–193 (2015).
242. Turner, S. J., Langmuir, C., Katz, R. F., Dungan, M. A. & Escrig, S. Parental arc magma compositions dominantly controlled by mantle-wedge thermal structure. *Nat. Geosci.* https://doi.org/10.1038/ngeo2788 (2016).
243. Gale, A., Dalton, C. A., Langmuir, C. H., Su, Y. & Schilling, J.-G. The mean composition of ocean ridge basalts. *Geochem. Geophys. Geosyst.* **14**, 489–518 (2013).
244. Nicklas, R. W., Puchtel, I. S. & Ash, R. D. Redox state of the Archean mantle: evidence from V partitioning in 3.5–2.4 Ga komatiites. *Geochim. Cosmochim. Acta* **222**, 447–466 (2018).
245. Shchipansky, A., Khodorevskaya, L. & Slabunov, A. The geochemistry and isotopic age of eclogites from the Belomorian belt (Kola Peninsula): evidence for subducted Archean oceanic crust. *Russian Geol. Geophys.* **53**, 262–280 (2012).
246. Guo, R. et al. Geochemistry, zircon U–Pb geochronology and Lu–Hf isotopes of metavolcanics from eastern Hebei reveal Neoarchean subduction tectonics in the North China Craton. *Gondwana Res.* **24**, 664–686 (2013).
247. Noack, N. M., Kleinschrodt, R., Kirchenbaur, M., Fonseca, R. O. C. & Münker, C. Lu–Hf isotope evidence for paleoproterozoic metamorphism and deformation of Archean oceanic crust along the Dharwar craton margin, southern India. *Precambrian Res.* **233**, 206–222 (2013).
248. Nikitina, L., Korolev, N., Zinchenko, V. & Felix, J. T. Eclogites from the upper mantle beneath the Kasai craton (Western Africa): petrography, whole-rock geochemistry and UPb zircon age. *Precambrian Res.* **249**, 13–32 (2014).
249. Malaspina, N. et al. The redox budget of crust-derived fluid phases at the slab-mantle interface. *Geochim. Cosmochim. Acta* **209**, 70–84 (2017).

Acknowledgements

The authors are grateful to have received constructive reviews that improved the manuscript. E.C. thanks their reading group and M. Brounce and F. Davis in particular for helpful discussions. D.C. is supported by an NSERC of Canada Discovery grant. F.G. acknowledges support from ANR grant agreement no. ANR-18-CE31-0021 'GASTON' and the ERC Synergy grant agreement no. 101166936 'GEOASTRONOMY'. K.A.E. acknowledgess funding from the Australian Research Council Discovery grant no. DP210101866.

Author contributions

E.C., D.C., C.L., K.A.E. and F.G. contributed to the conceptualization and writing. E.C., D.C. and K.A.E. contributed to writing of the original draft and visualization. E.C., D.C. and C.L. contributed to methodology and validation. E.C. and D.C. contributed to formal analysis and data curation. E.C. contributed to project administration.

Competing interests

The authors declare no competing interests.

Additional information

Supplementary information The online version contains supplementary material available at https://doi.org/10.1038/s43017-025-00735-1.

Peer review information *Nature Reviews Earth & Environment* thanks Claire Bucholz, Giulia Marras, Vincenzo Stagno and the other, anonymous, reviewer(s) for their contribution to the peer review of this work.